


RESEARCH

Open Access



ER Ca²⁺ overload activates the IRE1α signaling and promotes cell survival

Song Zhao^{1,4†}, Haiping Feng^{1,4†}, Dongfang Jiang^{1,4†}, Keyan Yang^{1,4}, Si-Tong Wang^{1,4}, Yu-Xin Zhang^{1,4}, Yun Wang¹, Hongmei Liu^{1,3*}, Caixia Guo^{2,4*} and Tie-Shan Tang^{1,3,4*} 

Abstract

Background Maintaining homeostasis of Ca²⁺ stores in the endoplasmic reticulum (ER) is crucial for proper Ca²⁺ signaling and key cellular functions. Although Ca²⁺ depletion has been known to cause ER stress which in turn activates the unfolded protein response (UPR), how UPR sensors/transducers respond to excess Ca²⁺ when ER stores are overloaded remain largely unclear.

Results Here, we report for the first time that overloading of ER Ca²⁺ can directly sensitize the IRE1α-XBP1 axis. The overloaded ER Ca²⁺ in TMCO1-deficient cells can cause BiP dissociation from IRE1α, promote the dimerization and stability of the IRE1α protein, and boost IRE1α activation. Intriguingly, attenuation of the over-activated IRE1α-XBP1 signaling by a IRE1α inhibitor can cause a significant cell death in TMCO1-deficient cells.

Conclusions Our data establish a causal link between excess Ca²⁺ in ER stores and the selective activation of IRE1α-XBP1 axis, underscoring an unexpected role of overload of ER Ca²⁺ in IRE1α activation and in preventing cell death.

Keywords ER Ca²⁺ overload, TMCO1, ER stress, IRE1α

Introduction

As a major intracellular Ca²⁺ store, the ER is essential for protein folding, secretion and Ca²⁺ homeostasis [1]. Environmental stressors, such as disruption of Ca²⁺ homeostasis, viral infection, and redox homeostasis,

lead to the accumulation of misfolded proteins in the ER, eliciting ER stress [2, 3]. To adapt to the disturbance of the external environment and reestablish ER homeostasis, the unfolded protein response (UPR) is triggered through three adaptive pathways mediated by the ER stress sensors, including inositol-requiring enzyme 1 (IRE1α/ERN1), activating transcription factor 6 (ATF6), and protein kinase RNA-like-ER kinase (PERK/EIF2AK3) [2, 4–8]. Under physiological conditions, the ER luminal domain of three stress effectors is associated with binding immunoglobulin protein (BiP) to maintain their inactive state [5, 9].

IRE1α is the most conserved and extensively studied UPR sensor protein [10, 11], which belongs to the type I transmembrane protein family, consisting of a luminal domain (LD), a single transmembrane domain, and a dual enzyme domain including a kinase domain (Kinase) and an endoribonuclease (RNase) domain in the cytosolic portion [3, 12]. Once activated, BiP is titrated away by unfolded proteins, leaving IRE1α free to initiate

[†]Song Zhao, Haiping Feng and Dongfang Jiang have contributed equally to this work.

*Correspondence:

Hongmei Liu
liuhongmei@ioz.ac.cn
Caixia Guo
guocx@big.ac.cn
Tie-Shan Tang
tangtsh@ioz.ac.cn

¹ State Key Laboratory of Membrane Biology, Institute of Zoology, Chinese Academy of Sciences, Beijing 100101, China

² Beijing Institute of Genomics, Chinese Academy of Sciences/China National Center for Bioinformation, Beijing 100101, China

³ Beijing Institute for Stem Cell and Regenerative Medicine, Beijing 100101, China

⁴ University of Chinese Academy of Sciences, Beijing 100049, China



dimerization-dependent autophosphorylation of its cytosolic domain. The subsequent allosteric activation of the cytosolic RNase domain triggers unconventional splicing of the mRNA encoding the transcription factor X-box binding protein 1 (XBP1), thereby promoting translation of the functional transcription factor, XBP1s (spliced XBP1). In turn, XBP1s then upregulates the transcription of conserved genes encoding ER-associated degradation (ERAD) components, chaperones, and folding enzymes to re-establish the ER proteostasis [5, 13–15]. Under severe or chronic ER stress, prolonged IRE1 α activation promotes apoptotic signaling downstream of the ASK-JNK axis and inflammatory signaling downstream of nuclear factor (NF κ B) by binding tumor necrosis factor receptor-associated factor 2 (TRAF2) to promote cell death [16, 17].

It is known that depletion of ER Ca²⁺ with the sarco-/endoplasmic-reticulum Ca²⁺-ATPase (SERCA) inhibitor thapsigargin (TG) can lead to ER dysfunction and to activate the UPR [2, 18]. To maintain efficient folding, the ER maintains an environment enriched in chaperones [19]. Previous studies have identified the Ca²⁺ binding potential of many chaperones, such as BiP, GRP94, and calreticulin, which act as buffer proteins for maintaining the ER Ca²⁺ homeostasis, while Ca²⁺ in turn is also important for the activity of these chaperones [20, 21]. ER Ca²⁺ depletion could significantly affect protein processing and then lead to the accumulation of unfolded proteins in the ER [22–24]. Most of the accepted models propose that BiP binds directly to the regulator lumen domain of the UPR sensors to keep them in an inhibited state [25, 26], while ER Ca²⁺ depletion-triggered accumulation of unfolded proteins can compete to bind BiP and thus to activate the UPR pathway [5, 25].

ER Ca²⁺ overload happens in multiple diseases including Alzheimer's disease [27–32], targeting of intracellular Ca²⁺ stores may have therapeutic potential for treating these diseases. However, whether and how UPR sensors/transducers respond to the excess Ca²⁺ when ER stores

are overloaded remains unclear. As an ER Ca²⁺ load-activated Ca²⁺ channel (CLAC), transmembrane and coiled-coil domains 1 (TMCO1) is important for maintaining ER Ca²⁺ homeostasis [33], whose deletion can cause ER Ca²⁺ overload. We and others have reported that TMCO1 deficiency can cause cerebrotendinous dysplasia (CFTD) [34], defects in bone formation [35] and defects in corpus callosum development [36]. In this study, we explored the effect of TMCO1 deficiency on ER stress signaling. We show that depletion of TMCO1 can activate IRE1 α by increasing its stability and oligomerization in a Ca²⁺-dependent manner. Moreover, the ER Ca²⁺ overfilling signaling directly sensitizes the IRE1 α -XBP1 axis, which is essential for modulating cell fate and helping cell survival.

Results

TMCO1 depletion boosts the activation of the IRE1 α -XBP1 pathway

To assess whether TMCO1 deficiency is linked to ER stress, we investigated the role of TMCO1 in the induction of the UPR. Interestingly, we found that knockdown (KD) of TMCO1 could increase the expression of IRE1 α and promote IRE1 α overactivation and XBP1 splicing (Additional file 1a and Fig. 1a), however, with no obvious effect on the expression of BiP and CHOP (Additional file 1a, b, c), two key factors involved in the ATF6 and PERK pathways of the UPR, respectively [15, 37]. In support of this, TMCO1 KD also significantly elevated the mRNA level of *Edem1*, a classical XBP1s target gene (Fig. 1b). To analyze the effects of TMCO1 deficiency on the UPR pathways more accurately, WT and KD cells were exposed to ER stressor TG. Supportingly, when cells were challenged by TG, TMCO1 KD boosted the activity of IRE1 α but not PERK and ATF6 (Fig. 1c). Given that KD of TMCO1 promotes IRE1 α expression and the RNase activity of IRE1 α , which can selectively degrade some mRNAs through a process known as regulated IRE1-dependent decay (RID) [38], we then examined

(See figure on next page.)

Fig. 1 TMCO1 knockdown leads to the overactivation of IRE1 α . **a–b** qRT-PCR analysis of Xbp1s/Xbp1u (**a**), and Edem1 (**b**) mRNA levels in WT or TMCO1 KD cells. Data are shown as mean \pm SEM from three independent experiments. n.s., no significance, * P < 0.05, ** P < 0.01. **c** Western blotting analysis of the UPR marker proteins, including p-PERK, PERK, p-eIF2 α , eIF2 α , ATF4, p-IRE1 α , IRE1 α , XBP1s and ATF6-N (N-terminal cleavage product of ATF6), in untreated or TG-treated (1 μ M, 4 h) WT and TMCO1 KD cells. GAPDH was used as a loading control. Relative quantification of each protein was shown in the right panel. Bar graphs represent the mean \pm SEM from three independent experiments. * P < 0.05, ** P < 0.01, n.s., no significance. **d** Western blotting analysis of proteins in WT and TMCO1 KD cells treated with/without 20 μ M KIRA6 for 24 h. GAPDH was used as a loading control. **e** Relative quantification of p-IRE1 α protein levels in D. Data are shown as the mean protein intensity normalized to GAPDH \pm SEM from 3 independent experiments. n.s., no significance, ** P < 0.01. **f** qRT-PCR analysis of Xbp1 mRNA splicing in WT and TMCO1 KD cells treated with/without 20 μ M KIRA6 for 24 h. Bar graphs represent the mean \pm SEM from three independent assays. ** P < 0.01, n.s., no significance. **g** FACS analysis of mCherry-positive cells. WT or TMCO1 KD cells were transfected with the UPR-mCherry. SSC-A: side-scatter area, which can indicate the granularity of the cell. Bar graph in the right panel represents the mean \pm SEM for mCherry-positive cells from three independent assays. *** P < 0.001. **h** Western blotting analysis of p-IRE1 α and IRE1 α levels in WT and TMCO1 KD cells transfected with control mCherry vector or TMCO1-IRES-mCherry. Tubulin was used as a loading control. Relative quantification of protein levels is shown in the right panel. Data are shown as the mean protein intensity normalized to tubulin \pm SEM from 3 independent experiments. * P < 0.05, ** P < 0.01

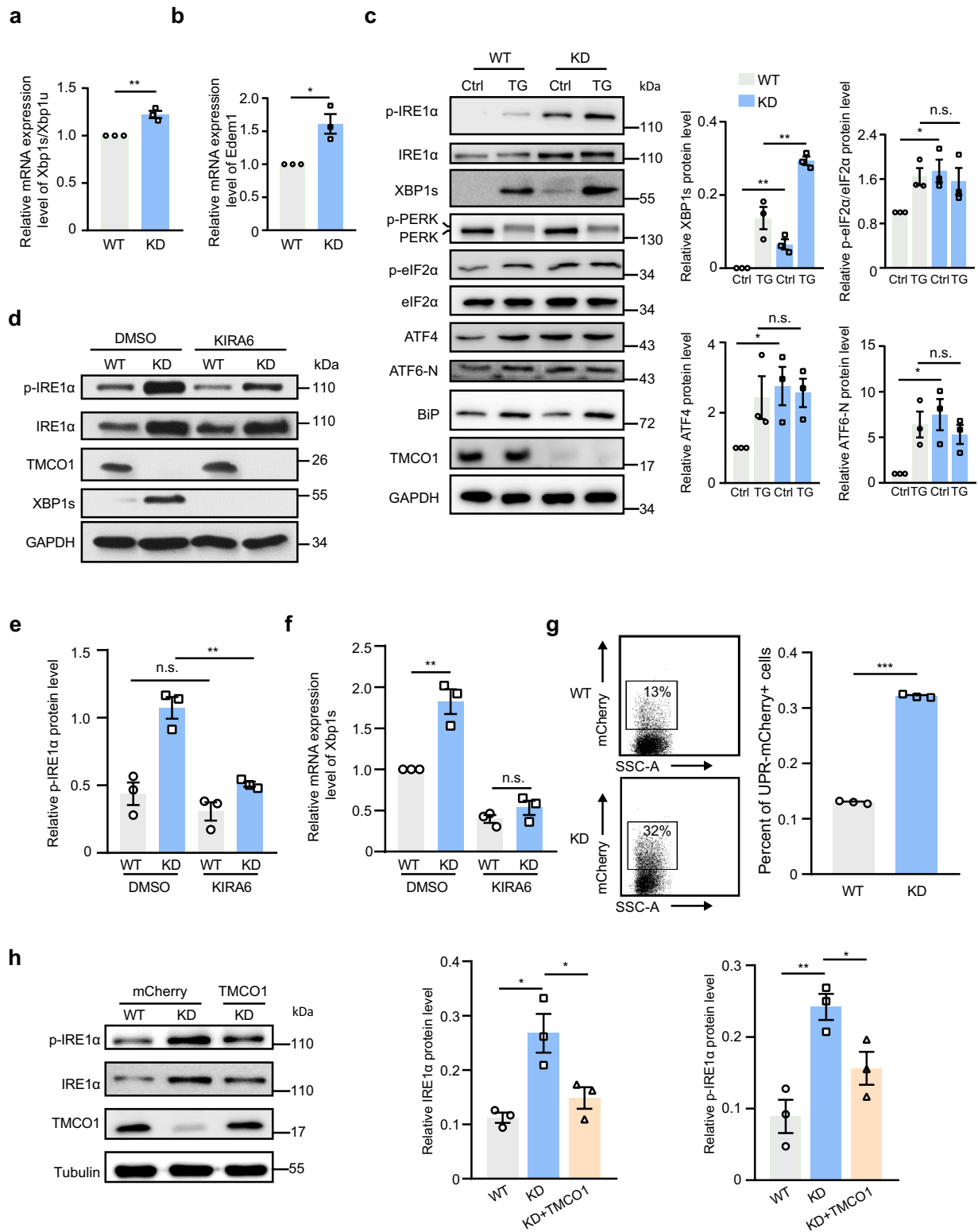


Fig. 1 (See legend on previous page.)

the mRNA level of a RIDD target gene SPARC [39, 40]. We found that its expression was significantly down-regulated in KD cells (Additional file 1d). These results indicate that TMCO1 depletion can lead to an active ER stress pathway mediated mainly by IRE1 α but not PERK or ATF6.

To further explore the association of TMCO1 loss with IRE1 α -mediated UPR, we treated TMCO1 wild-type (WT) and KD HeLa cells with an IRE1 α inhibitor KIRA6 [41]. We found that KIRA6 treatment markedly reduced the levels of IRE1 α phosphorylation and XBP1s in KD cells with no obvious effect on IRE1 α expression (Fig. 1d, e, f), indicating that TMCO1 KD directly activates both the kinase and RNase activities of IRE1 α . To detect cellular ER stress-induced IRE1 α activation directly, we then constructed a UPR-mCherry reporter with the UPR response element (UPRE), which can drive mCherry expression through XBP1s production, thus reflecting IRE1 α activation specifically [42, 43]. The reporter was transfected into HEK-293 T cells followed by treatment with either TG (to induce ER stress) or 4 μ 8C (a specific IRE1 α RNase inhibitor) [44]. The quantity of TG used for the cell treatment was calibrated first to avoid excessive XBP1 splicing, and a concentration of 1 μ M TG for a 2 h incubation was defined for ER stress stimulation, as no significant difference of spliced XBP1s levels was observed between WT and KD under this condition (Additional file 1e). We found that TG treatment significantly stimulated the expression of XBP1s and mCherry compared to the DMSO control, while supplementation with 4 μ 8C largely blocked the stimulatory effect, indicating that this UPR-mCherry reporter we prepared could be used to indicate the ER stress-induced IRE1 α activation in cells (Additional file 1f) as previously reported. We then transfected the UPR-mCherry reporter into WT and KD cells and detected a significant increase in the mCherry signal in KD cells compared to WT cells (Fig. 1g), supporting that TMCO1 loss can boost ER

stress-induced IRE1 α activation. ER Ca²⁺ overload and activation of IRE1 α induced by knockdown of TMCO1 were also verified in HEK-293 T cells (Additional file 1 g, h, i).

To further support that the overactivation of IRE1 α in TMCO1 KD cells is indeed caused by TMCO1 depletion, a TMCO1-IRES-mCherry construct was transfected back into the TMCO1 KD cells. We found that expressing TMCO1-IRES-mCherry but not mCherry in KD cells could attenuate the increase in IRE1 α expression and its phosphorylation (Fig. 1h). Taken together, these results indicate that TMCO1 plays an important regulatory role in IRE1 α -XBP1s pathway activation.

TMCO1 regulates the activation of IRE1 α depending on Ca²⁺ signaling

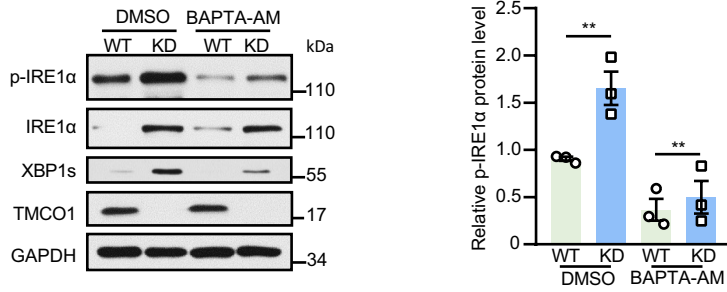
We then investigated how TMCO1 regulates the IRE1 α -XBP1s activation. Considering TMCO1 depletion can cause an ER Ca²⁺ overload, we wonder whether the abnormal Ca²⁺ signaling plays a role in IRE1 α overactivation in KD cells. Using BAPTA-AM, an intracellular Ca²⁺ chelator, to treat WT and KD cells, we noted that the overactivation of IRE1 α phosphorylation and increased expression of XBP1s protein in KD cells were largely abrogated (Fig. 2a), indicating that the overactivation of IRE1 α caused by TMCO1 deficiency is likely attributed to altered Ca²⁺ levels.

To determine whether TMCO1 depletion could sensitize the IRE1 α -XBP1 pathway upon ER stress induction, and whether alteration of Ca²⁺ level is involved in this process, WT and KD cells were exposed to three distinct ER stressors independently, including tunicamycin (TM), TG or DTT, in the presence or absence of BAPTA-AM. We found that treatments with these ER stressors could significantly increase the mRNA (Fig. 2b, d, f) and protein (Fig. 2c, e, g) levels of XBP1s in both WT and KD cells, with a more pronounced increase in KD cells compared to WT cells. Interestingly, concurrent treatment with

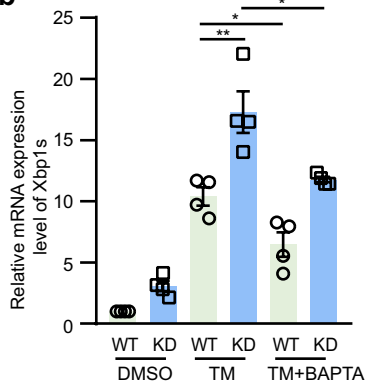
(See figure on next page.)

Fig. 2 TMCO1 KD enhances IRE1 α -XBP1 pathway in a Ca²⁺ dependent manner. **a** Western blotting analysis of p-IRE1 α , IRE1 α and XBP1s levels in WT and TMCO1 KD cells treated with/without 50 μ M BAPTA-AM for 2 h. Relative quantification of p-IRE1 α level is shown in the right panel. Data are shown as the mean protein intensity normalized to GAPDH \pm SEM from 3 independent experiments. ** P < 0.01. **b** qRT-PCR analysis of Xbp1 mRNA splicing in WT and TMCO1 KD cells treated with 3 μ g/ml TM along with/without 50 μ M BAPTA-AM for 4 h. Bar graphs represent the mean \pm SEM from three independent assays. * P < 0.05; ** P < 0.01. **c** The levels of XBP1s in WT and TMCO1 KD cells were measured by western blotting analysis after the treatment of 3 μ g/ml TM along with/without 50 μ M BAPTA-AM for 4 h. GAPDH was used as a loading control. Relative quantification of XBP1s levels was shown in the right panel. Data are shown as the mean protein intensity normalized to GAPDH \pm SEM from 3 independent experiments. * P < 0.05, ** P < 0.01, *** P < 0.001. **d** qRT-PCR analysis of Xbp1 mRNA splicing in WT and TMCO1 KD cells treated with 1 μ M TG along with/without 50 μ M BAPTA-AM for 4 h. Bar graphs represent the mean \pm SEM from three independent assays. ** P < 0.01, *** P < 0.001. **e** The levels of XBP1s in WT and TMCO1 KD cells were measured (Left) and quantified (Right) by western blotting after the treatment of 1 μ M TG along with/without 50 μ M BAPTA-AM for 4 h. GAPDH was used as a loading control. Data are shown as the mean protein intensity normalized to GAPDH \pm SEM from 3 independent experiments. * P < 0.05, ** P < 0.01, *** P < 0.001. **f** qRT-PCR analysis of Xbp1 mRNA splicing in WT and TMCO1 KD cells treated with 5 mM DTT along with/without 50 μ M BAPTA-AM for 4 h. Bar graphs represent the mean \pm SEM from three independent assays. * P < 0.05; ** P < 0.01, *** P < 0.001. **g** The levels of XBP1s in WT and TMCO1 KD HeLa cells were measured (Left) and quantified (Right) by western blotting analysis after the treatment of 5 mM DTT along with/without 50 μ M BAPTA-AM for 4 h. GAPDH was used as a loading control. Data are shown as the mean protein intensity normalized to GAPDH \pm SEM from 3 independent experiments. ** P < 0.01, *** P < 0.001

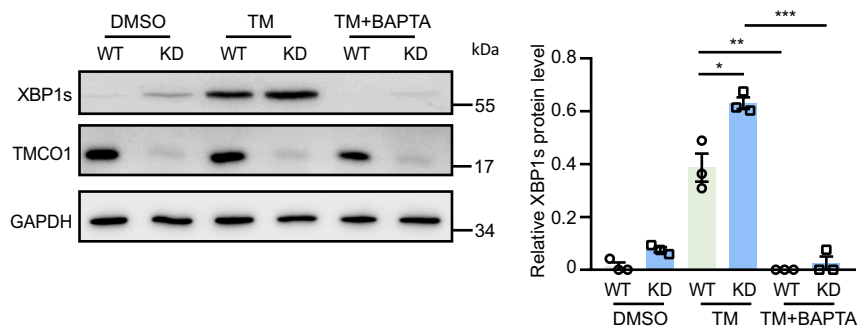
a



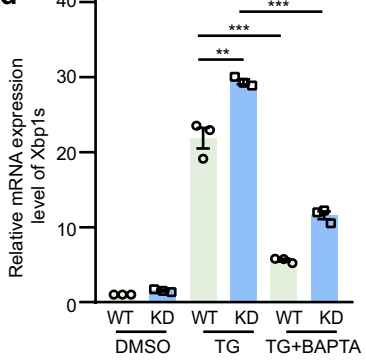
b



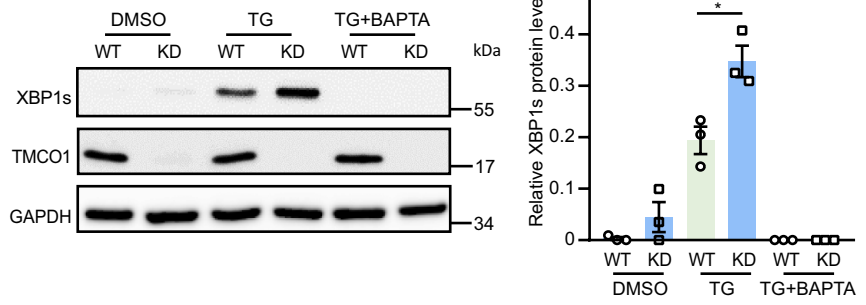
c



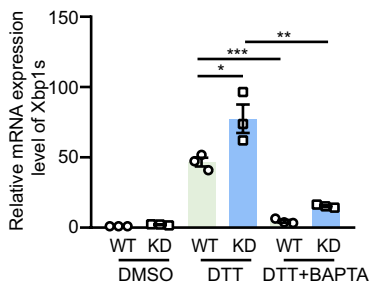
d



e



f



g

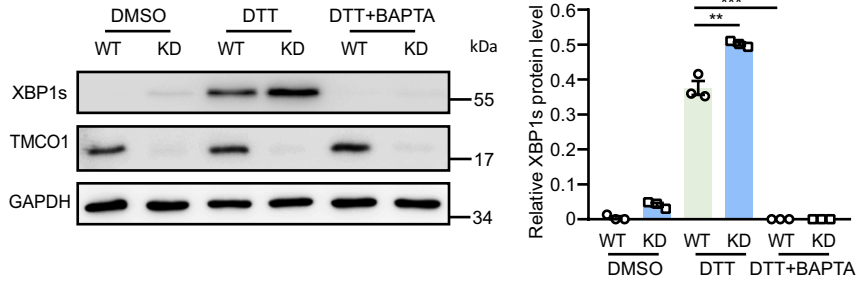


Fig. 2 (See legend on previous page.)

BAPTA-AM almost completely abolished the increase of XBP1s caused by ER stressors. These data demonstrate that TMCO1 deficiency can enhance the IRE1 α -XBP1 axis in a Ca²⁺ signaling-dependent manner. Additionally, we observed that the effect of BAPTA-AM on XBP1s protein level was far greater than that on its mRNA level, which could be due to the direct effect of BAPTA-AM on protein synthesis by upregulating phosphorylation of the translational initiation factor eIF2 α [45], resulting in a suppression of the initiation step of protein synthesis. We also demonstrated that BAPTA-AM could repress global translation (Additional file 2a). Thus, it is likely that BAPTA-AM inhibits the translation of XBP1s.

ER Ca²⁺ overfilling sensitizes the IRE1 α -XBP1 axis

Although TM, DTT and TG treatment could sensitize the IRE1 α -XBP1 pathway in a Ca²⁺ signaling-dependent manner in KD cells, it is unclear whether this sensitization effect was caused by the overfilling of ER Ca²⁺ or the release of excessive Ca²⁺ into the cytoplasm from ER. Our findings that TG, an ER stressor that can deplete ER luminal Ca²⁺ [46], but not TM and DTT, a reducing agent that prevents disulfide bond formation of ER nascent proteins [47], caused a transient release of Ca²⁺ from the ER (Additional file 2b, c), provide preliminary evidence of the involvement of ER Ca²⁺ in this process. We therefore speculated that the overfilling of Ca²⁺ in the ER caused by TMCO1 depletion might affect the IRE1 α activation. To support this notion, different Ca²⁺ inducers other than TG, including ATP, ionomycin (iono) and carbachol (Cch), were used to treat WT and KD cells, and then the cytosolic Ca²⁺ was measured by the Ca²⁺ indicator fura-2. Significantly higher amplitudes of Ca²⁺ transients were detected in KD cells than in WT cells upon treatment with these Ca²⁺ inducers (Additional file 3a, b, c). Moreover, the overfilling state of the ER Ca²⁺ store was further confirmed by the mKate-linker-G-CEPIA1er (miGer) [48] in KD cells (Additional file 3d). Together,

these results confirm that TMCO1 deficiency indeed causes overfilling of ER Ca²⁺ store.

We then explored the role of ER Ca²⁺ overfilling in the activation of IRE1 α . Based on our previous results [33], a TMCO1 mutant (D140A) lacking the Ca²⁺ permeation function was constructed. We found that the increased Ca²⁺ release after TG treatment in KD cells could be rescued by the expression of WT TMCO1 but not the D140A mutant, demonstrating that the regulation of Ca²⁺ signaling by TMCO1 depends on its Ca²⁺ permeability (Fig. 3a, b). Interestingly, we found that exogenous expression of WT TMCO1 but not the D140A mutant could rescue the phosphorylation level of IRE1 α (Fig. 3c) and the expression of XBP1s in KD cells (Fig. 3c, d). These data clearly show that the overload of ER Ca²⁺ is critical for the regulatory role of TMCO1 in IRE1 α activation, and the activation of IRE1 α is closely linked to the Ca²⁺ overfilling state in the ER instead of the TMCO1 protein itself.

Overload of ER Ca²⁺ disrupts the interaction between BiP and IRE1 α

We next investigated how the overload of ER Ca²⁺ affects the IRE1 α activation. BiP is a negative regulator of IRE1 α , whose dissociation from the luminal domain (LD) of IRE1 α is required for IRE1 α activation [49, 50]. Consistent with previous results [51], deletion of the LD (resides 30-407) in IRE1 α attenuated IRE1 α phosphorylation and XBP1 splicing (Fig. 4a), supporting that the LD of IRE1 α was important for IRE1 α activation. Normally, the activation of the UPR pathway induced by the accumulation of unfolded proteins in ER leads to the elevation of chaperones in response to the excessive accumulation of unfolded proteins in ER. However, the expression of both BiP (Additional file 1a) and calnexin, another ER resident chaperone with a high capacity for Ca²⁺ binding [52, 53] remained unchanged when TMCO1 was knocked down (Fig. 4b), indicating that no accumulation of large

(See figure on next page.)

Fig. 3 Over-activation of IRE1 α induced by TMCO1 knockdown is dependent on Ca²⁺ rather than the TMCO1 protein. **a** Representative images of Fura-2 340/380 ratios in WT, TMCO1 KD cells and TMCO1 KD cells transfected with TMCO1 or TMCO1-D140A-IRES-mCherry. Ratios were recorded for 1 μ M TG-induced Ca²⁺ transients in these cells. The pseudo-color calibration scale for 340/380 ratios was shown on the right. mCherry images (first column) were captured before TG-induced Ca²⁺ imaging to identify TMCO1 expressing cells. Representative images were shown for cells 30 s before (second column), and 45 s, 75 s, 120 s, and 240 s after application of 1 μ M TG as indicated. Scale bar, 20 μ m. **b** Left panel, 1 μ M TG-triggered Ca²⁺ transients in WT transfected with IRES-mCherry (purple trace line, n = 124), TMCO1 KD transfected with IRES-mCherry (red trace line, n = 76), TMCO1 KD cells transfected with TMCO1-IRES-mCherry (green trace line, n = 62), TMCO1 KD cells transfected with TMCO1-D140A-IRES-mCherry (blue trace line, n = 173). Each trace line in B is an average of Ca²⁺ responses from all mCherry-positive cells in each group. Right panel, statistical analysis of the average peak area of 1 μ M TG-triggered Ca²⁺ mobilization curves. Bar graphs represent the mean \pm SEM from three independent assays. ****P < 0.001. **c** Western blotting analysis of p-IRE1 α , IRE1 α and XBP1s levels in WT, TMCO1 KD cells, TMCO1 KD cells transfected with TMCO1 or TMCO1-D140A-IRES-mCherry. GAPDH was used as a loading control. Relative quantification of each protein levels was shown in the right panel. Bar graphs represent the mean \pm SEM from three independent experiments. **P < 0.01, ***P < 0.001, n.s., no significance. **d** qRT-PCR analysis of Xbp1 mRNA splicing in WT, TMCO1 KD HeLa cells, TMCO1 KD HeLa cells transfected with TMCO1 or TMCO1-D140A-IRES-mCherry. Bar graphs represent the mean \pm SEM from three independent assays. **P < 0.01, ***P < 0.001, n.s., no significance

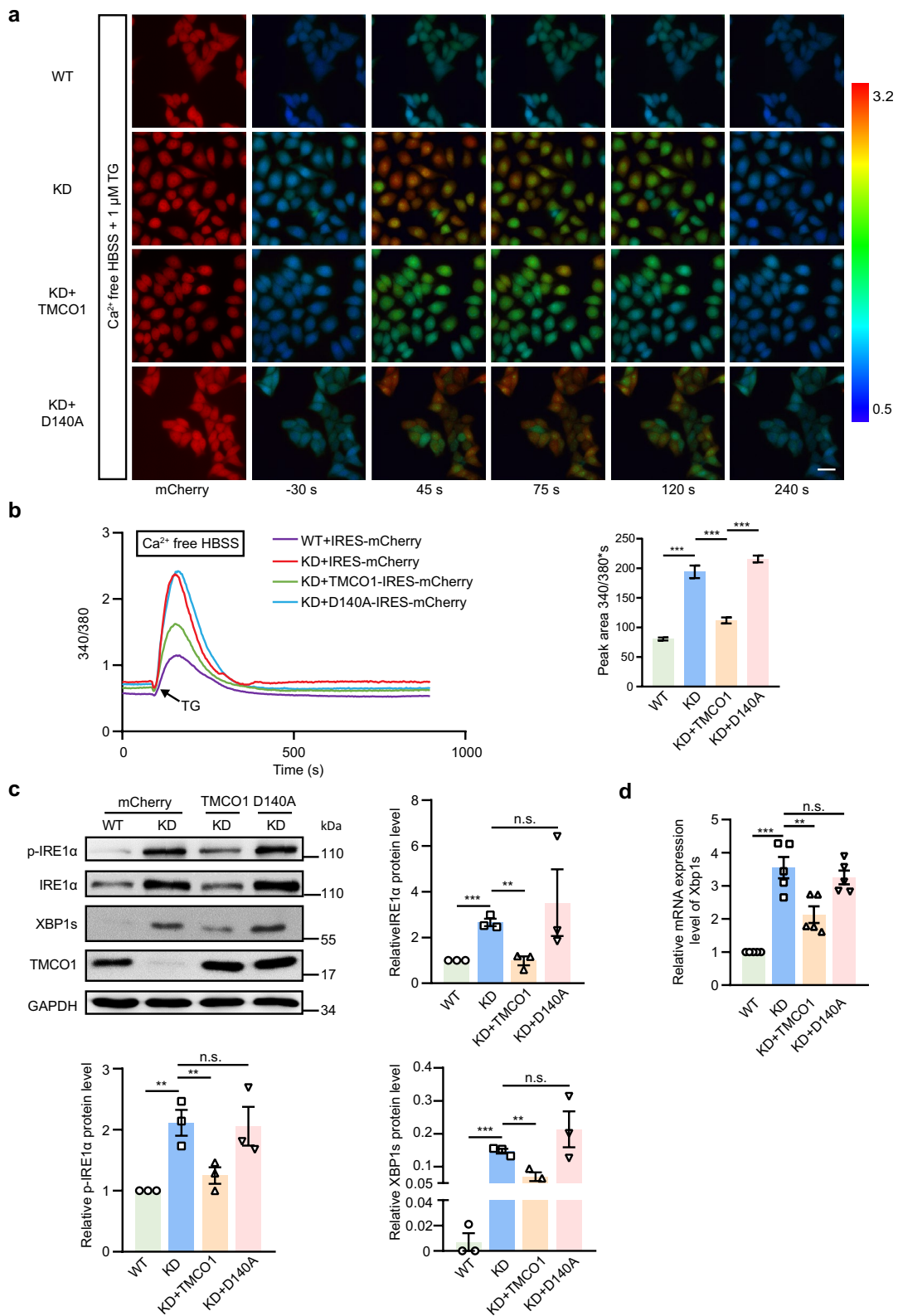


Fig. 3 (See legend on previous page.)

amounts of unfolded protein in the ER occur upon TMCO1 depletion.

We then examined whether ER Ca^{2+} overload could affect the interaction between BiP and IRE1 α . Previous studies have reported that the association between BiP and IRE1 α is mediated by the nucleotide binding domain in BiP and the LD of IRE1 α in a nucleotides-independent manner [54, 55]. We therefore purified both the GST-tagged BiP-nucleotide binding domain (NBD) and Flag-tagged IRE1 α -LD separately followed by GST pull-down experiment in the presence of different concentrations of Ca^{2+} . As the estimated Ca^{2+} concentration in the ER lumen is around 0.5 to 0.8 mM in the resting state [26, 56], three different concentrations of Ca^{2+} , that is, 0.5, 0.8 and 1.2 mM, were used in the pull-down assay. Our result showed that the interaction between BiP-NBD and IRE1 α -LD could only be disrupted by 1.2 mM Ca^{2+} but not by 0.8/0.5 mM Ca^{2+} (Fig. 4c), indicating that the binding of NBD to IRE1 α 's luminal domain is dependent on Ca^{2+} and that only Ca^{2+} beyond the physiological range could disrupt the interaction between BiP and IRE1 α .

To support that, we also examined the effect of a simulated ER Ca^{2+} overload environment on the interaction between BiP and IRE1 α . To that end, HEK-293 T cells were treated with CDN1163, a pharmacologic agent known to increase ER Ca^{2+} levels by inducing SERCA pump activation [53], or 2-APB, an antagonist that blocks the exit of ER Ca^{2+} by antagonizing IP $_3$ Rs [57], with TG as a negative control. As expected, TG reduced ER Ca^{2+} levels, whereas CDN1136 and 2-APB increased ER Ca^{2+} levels (Fig. 4d, e). Our immunoprecipitation results showed that BiP interacted with IRE1 α rather than TMCO1 in the resting state, and TG or CDN1136/2-APB treatment significantly reduced the association of BiP to IRE1 α (Fig. 4f, g), indicating that either depletion or overload of Ca^{2+} in the ER can reduce the interaction of BiP with IRE1 α . Taken together, these results reveal that ER Ca^{2+} overload caused by depletion of TMCO1 can

reduce the binding of BiP to IRE1 α and boost the activation of IRE1 α .

ER Ca^{2+} overfilling enhances the stability and oligomerization of IRE1 α

Since KD of TMCO1 could increase the expression of IRE1 α (Additional file 1a), we then explored the underlying mechanism. To determine whether the increased IRE1 α expression was due to its enhanced transcription, KD cells were treated with actinomycin D (ACTD), an inhibitor of RNA synthesis [58, 59]. qPCR and western blotting results showed that ACTD treatment significantly decreased the transcription of IRE1 α (Fig. 5a), while the increased IRE1 α expression at protein levels could still be detected in TMCO1 KD cells (Fig. 5a, b), suggesting that TMCO1 depletion may promote IRE1 α protein stability at the post-transcriptional level. To determine whether TMCO1 depletion can promote IRE1 α expression at the protein level, we treated WT and KD cells with cycloheximide (CHX), a widely used protein synthesis inhibitor in eukaryotic cells [60]. We found that the half-life of IRE1 α protein was dramatically increased in TMCO1 KD cells (Fig. 5c), demonstrating that depletion of TMCO1 can markedly enhance the stability of IRE1 α protein. It has been reported that IRE1 α protein can undergo dimer/oligomerization and is stabilized under ER stress [61, 62]. To examine whether the oligomerization of IRE1 α was related to the increased stability of IRE1 α caused by TMCO1 depletion, cells were treated with CHX in the presence or absence of KIRA6, which could prevent IRE1 α oligomerization. We found that the half-life of IRE1 α was dramatically decreased in KD cells after treatment with KIRA6 (Fig. 5d), providing evidence for the involvement of IRE1 α oligomerization in its enhanced stability. We next analyzed IRE1 α oligomerization in TMCO1-deficient cells by Blue Native polyacrylamide gel electrophoresis (BN-PAGE) immunoblotting [62]. The results showed that knockdown of TMCO1 significantly increased IRE1 α

(See figure on next page.)

Fig. 4 ER Ca^{2+} overload reduces the interaction between IRE1 α and BiP. **a** The levels of XBP1s in HEK293T-IRE1 α knockout cells transfected with IRE1 α or IRE1 α deleted LD were measured after treating with 1 μM TG for 2 h, followed by western blotting analysis. GAPDH was used as a loading control. Relative quantification of XBP1s levels was shown in the right panel. Data are shown as the mean protein intensity normalized to GAPDH \pm SEM from 3 independent experiments. *** P < 0.001. EV, empty vector. Δ LD, deleted LD of IRE1 α . **b** Expression levels of calnexin were analyzed by western blotting in the wild-type or TMCO1 KD cells. GAPDH was used as a loading control. **c** Pull down assay assessing the effects upon addition of increasing concentrations of Ca^{2+} to GST-tagged BiP-NBD and FLAG-tagged IRE1 α -LD complex. 1.2 mM Ca^{2+} disrupted IRE1 α -luminal domain interaction and causes the BiP-ATPase domain to dissociate. Relative quantification of LD-FLAG level was shown in the right panel. Data are shown as mean \pm SEM from three independent experiments. Statistical analysis was performed using one-way ANOVA with Tukey's multiple comparison test: *** P < 0.001. **d** The resting G-CEPIA1er fluorescence ratio signals were detected in HEK293T treated with 1 μM TG or 5 μM CDN1136 for 2 h. Ctrl, n = 103. TG, n = 171. CDN1136, n = 160. Bar graphs represent the mean \pm SEM from three independent assays. *** P < 0.001. **e** The resting G-CEPIA1er fluorescence ratio signals were detected in HEK-293 T treated with/without 100 μM 2-APB for 2 h. Ctrl, n = 105. 2-APB, n = 165. Bar graphs represent the mean \pm SEM from three independent assays. *** P < 0.001. **(f and g)** HEK-293 T cells transfected with BiP-Flag were treated with 1 μM TG or 5 μM CDN1136 **(f)** or 100 μM 2-APB **(g)** for 2 h followed by a co-immunoprecipitation for Flag. Protein loading was normalized to FLAG and relative co-immunoprecipitated IRE1 α was examined via immunoblotting

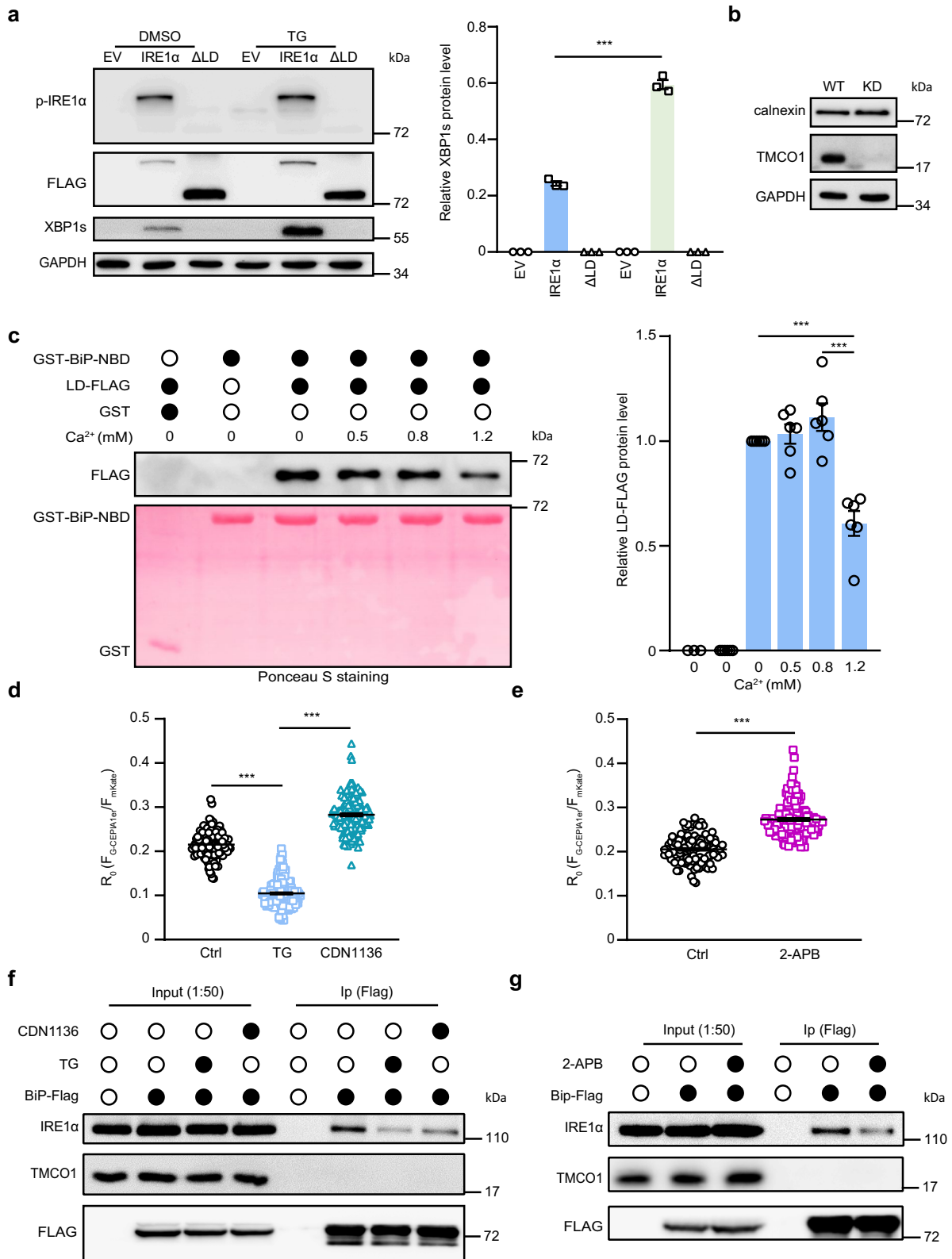


Fig. 4 (See legend on previous page.)

oligomerization, which could be completely reverted by WT TMCO1 but not the D140A mutant (Fig. 5e), revealing a Ca^{2+} -dependent enhancement of IRE1 α oligomerization in KD cells. Furthermore, consistent with the IRE1 α oligomerization results, the increased half-life of IRE1 α protein in KD cells was dramatically decreased by WT TMCO1 but not by the D140A mutant (Fig. 5f). Together, our results support that the IRE1 α stability and its dimerization/oligomerization are regulated by overload of ER Ca^{2+} when TMCO1 get depleted.

Tmco1 deficiency enhances IRE1 α signaling under ER stress in vivo

IRE1 α activation has been reported to enhance the susceptibility of cells to apoptosis. In view of the pro-survival properties of XBP1 splicing [1], we set out to test whether IRE1 α activation induced by TMCO1 deficiency could promote cell survival. WT and KD cells were treated with KIRA6 for 24 h and then the early apoptotic, late apoptotic, and dead cells were quantified by flow cytometry using Annexin V/PI. The results showed that although TMCO1 knockdown could promote cell death to a certain level, inhibiting the IRE1 α pathway by KIRA6 significantly boosted cell death, with a significant more effect in KD cells than WT cells (Fig. 6a, b). Specifically, KD cells induced a significantly higher percentage of both early and late apoptotic (necrotic stage) cells compared with WT cells under basal conditions, whereas upon KIRA6 treatment, KD lead to significantly more late apoptotic cells than WT. Consistent with annexin V-FITC+PI staining results, the level of RIPK1, an important mediator of necrosis [63] was also significantly elevated in KD cells in the presence of KIRA6 compared to the control cells (Fig. 6c). These results indicate that the potentiation of IRE1 α -XBP1 axis could help cell survival when ER Ca^{2+} get overloaded in KD cells.

To test the effect of TMCO1 on IRE1 α signaling in vivo, *Tmco1*^{+/+} and *Tmco1*^{-/-} mice at 2 months of age were intraperitoneally injected with a single dose of TM to trigger a strong UPR reaction in livers [1, 64–68].

Mice were sacrificed at 8, 16 or 24 h after TM injection for comparison of IRE1 α signaling activation in the liver. Consistent with previous studies [66], the highest amounts of XBP1s were observed at 8 h at both mRNA (Additional file 4a) and protein (Additional file 4b) levels, suggesting a decay of the TM-induced XBP1 splicing occurs in vivo. Therefore, the following analysis of IRE1 α signaling in the liver was performed at 8 h after TM injection. Our results showed that both the mRNA and protein levels of XBP1s were increased after TM treatment, with a bigger increase in *Tmco1*^{-/-} mice compared to WT mice (Fig. 6d, e). However, when analysis of the mRNA levels of genes involved in other UPR downstream signaling pathways, including *Bloc1s1*, *Bip* and *Chop*, was performed in WT and *Tmco1*-deficient livers, no significant change was detected under basal and TM treated situations (Fig. 6f). These results support that TMCO1 deficiency specifically enhances the IRE1 α -XBP1 pathway under ER stress conditions in vivo. Furthermore, we also assessed the damage effect of the TM injection in the liver tissue. Both hematoxylin and eosin (H&E) staining as well as picrosirius red staining showed that there were no signs of hepatocyte damage in *Tmco1*^{+/+} and *Tmco1*^{-/-} mice, indicating that the dose of TM used to treat mice did not cause liver damage at the histological level (Fig. 6g and Additional file 4c). Interestingly, although TMCO1 deficiency failed to upregulate basal ER stress in livers from 2-month-old mice, we detected a significant increase of XBP1s in the liver of 8-month-old *Tmco1*^{-/-} mice compared with age-matched WT mice (Additional file 4d). Given that the pro-survival properties of XBP1s could ameliorate Alzheimer's disease by improving synaptic function and proteostasis and protect against obesity-linked metabolic deterioration [37, 69], it is plausible that the activation of XBP1s in 8-month-old *Tmco1*^{-/-} mice may promote cell survival during mouse aging. Taken together, our results show that TMCO1 depletion boost the activation of the IRE1 α -XBP1 pathway under ER stress to promote cell survival in vivo.

(See figure on next page.)

Fig. 5 The dimerization and stability of IRE1 α regulated by TMCO1 depends on the overload of ER Ca^{2+} store. **a** qRT-PCR analysis of IRE1 α mRNA in WT or TMCO1 KD cells treated with/without 2.5 μM ACTD for 5 h. Bar graphs represent the mean \pm SEM from three independent assays. ****** $P < 0.01$, ******* $P < 0.001$. **b** Western blotting analysis of IRE1 α levels in WT and TMCO1 KD cells treated with/without 2.5 μM ACTD for 5 h. GAPDH was used as a loading control. Relative quantification of IRE1 α levels was shown in the right panel. Bar graphs represent the mean \pm SEM from three independent experiments. *** $P < 0.05$; ** $P < 0.01$** . **c** The stability of IRE1 α was measured after the treatment of 100 $\mu\text{g}/\text{ml}$ CHX for the indicated times, followed by western blotting analysis. GAPDH was used as a loading control. Relative quantification of IRE1 α levels was shown in the right panel. Bar graphs represent the mean \pm SEM from three independent experiments. *** $P < 0.05$, *** $P < 0.01$** . **d** The stability of IRE1 α was measured after the treatment of 100 $\mu\text{g}/\text{ml}$ CHX along with/without 20 μM KIRA6 for the indicated times, followed by western blotting analysis. GAPDH was used as a loading control. Relative quantification of IRE1 α levels was shown in the right panel. Bar graphs represent the mean \pm SEM from three independent experiments. *** $P < 0.05$, n.s., no significance**. **e** The digitonin lysate of WT, TMCO1 KD cells, TMCO1 KD cells transfected with TMCO1 or TMCO1-D140A-IRES-mCherry were analyzed by BN-PAGE immunoblotting with IRE1 α antibody. GAPDH was used as a loading control. **f** The stability of IRE1 α in WT, TMCO1 KD cells. TMCO1 KD cells transfected with TMCO1 or TMCO1-D140A-IRES-mCherry were treated with 100 $\mu\text{g}/\text{ml}$ CHX for the indicated times, followed by immunoblotting. GAPDH was used as a loading control

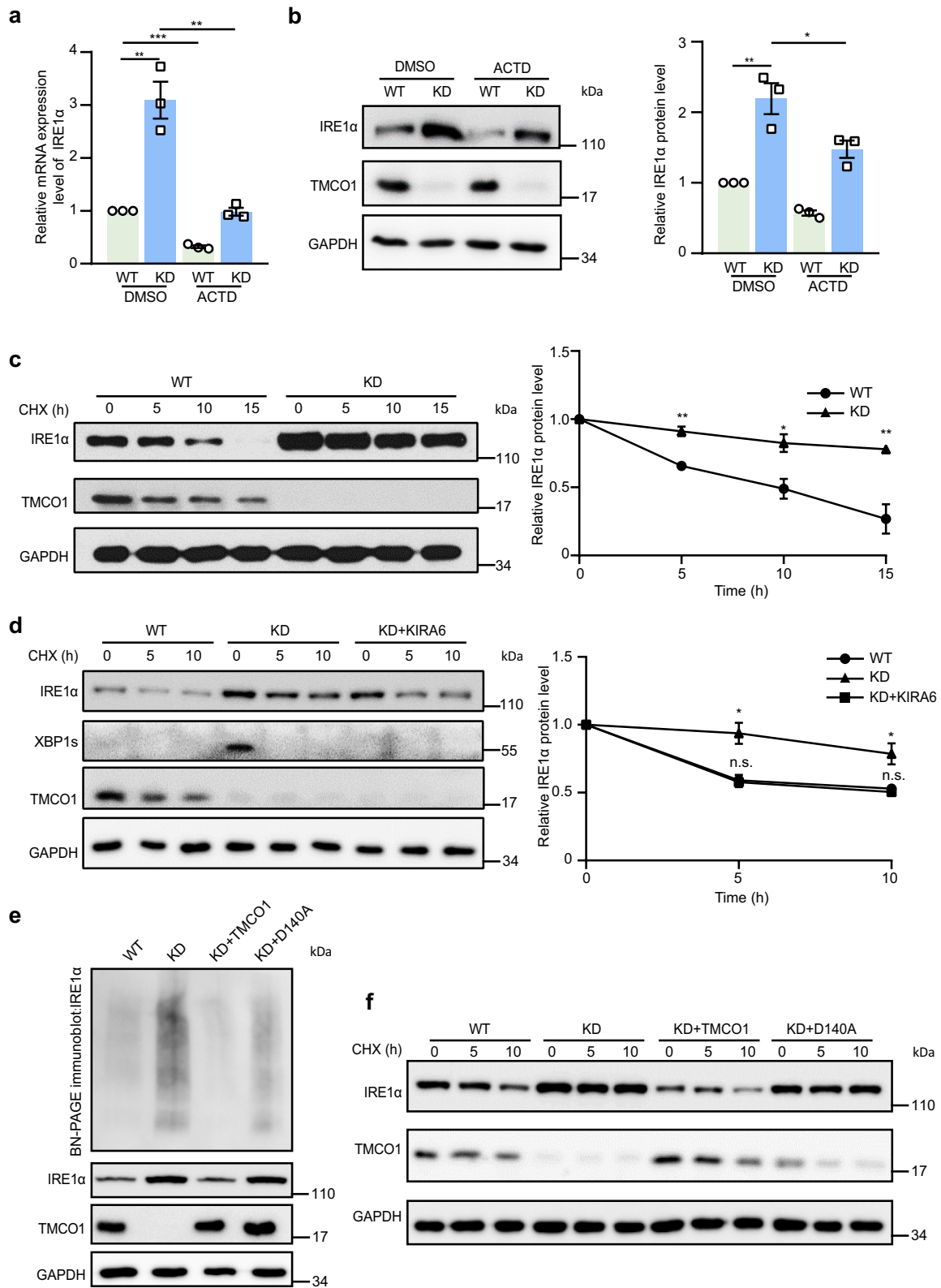


Fig. 5 (See legend on previous page.)

Discussion

IRE1 α is the most conserved and well-studied UPR sensor, which determines cell fate under ER stress derived from many factors, including inflammation, oxidative stress, glucose deprivation and aberrant Ca²⁺ regulation [70, 71]. IRE1 α expression is therefore under stringent regulation in vivo. Here, we identified TMCO1 as a novel regulator of IRE1 α . Based on our results that TMCO1 deficiency can cause the overload of ER Ca²⁺, which then disrupts the interaction between BiP and IRE1 α , we propose that the reduced interaction after TMCO1 depletion promotes the dimerization and stability of IRE1 α so that IRE1 α easily reaches a priming state in response to possible external stimuli to promote cell survival (Fig. 7). Our findings highlight a new way of regulating IRE1 α by TMCO1, and establish a causal link between excess Ca²⁺ in ER stores and the selective activation of IRE1 α -XBP1 axis.

Maintaining homeostasis of Ca²⁺ stores in the ER is crucial for proper Ca²⁺ signaling and key cellular functions such as protein synthesis, folding and maturation. ER Ca²⁺ homeostasis is modulated by Ca²⁺ binding proteins (e.g., calreticulin, BiP, and GRP94), ER-resident Ca²⁺ transporters, and Ca²⁺ channels, including ryanodine receptors (RyRs), ER-resident inositol 1,4,5-trisphosphate receptor (IP₃Rs), and SERCA [72–75]. It is known that ER Ca²⁺ depletion caused by SERCA inhibitors, such as TG, can trigger a robust activation of ER stress [76, 77]. Of note, alterations in ER Ca²⁺ homeostasis include not only Ca²⁺ depletion but also Ca²⁺ overfilling, with the latter being also an important ER Ca²⁺ homeostatic feature. However, it is still unclear whether ER Ca²⁺ overload induces ER stress. We previously reported that deficiency of TMCO1 in mouse granulosa cells could activate ER stress mainly mediated by the activities of the IRE1 α pathway [78], it is still unclear whether the effect is cell type-specific and related to ER Ca²⁺ overload. Here in this study, using in vitro and in vivo mouse model of ER stress, we have demonstrated that the overloading ER Ca²⁺ caused by TMCO1 depletion directly sensitizes the IRE1 α -XBP1 axis. Therefore, our findings underscore

an unexpected role of overload of ER Ca²⁺ in ER stress regulation.

Despite disagreements over details, most UPR regulatory models acknowledge the importance of BiP-substrate interactions [25]. It is well recognized that BiP binds to the UPR sensors to restrict it in an inhibited state [79, 80]. Under the condition of ER stress, unfolded proteins replace BiP from UPR sensors, leading to their activation [54]. The components of the ER protein folding machinery, including calnexin [26, 81], calreticulin [82], Grp94 [83, 84] and PDI, are known to have low-affinity Ca²⁺-binding sites, whose occupancy is likely decreased upon ER Ca²⁺ depletion within the physiological range [26]. Therefore, ER Ca²⁺ depletion is expected to favor the dissociation of BiP from UPR sensors [26, 85]. However, TMCO1 deficiency did not result in an increased expression of chaperones in the ER (Additional file 1a and Fig. 4b). Distinct from the fashion that ER Ca²⁺ depletion activates UPR sensors through accumulation of unfolded proteins in the ER, activation of UPR sensors by ER Ca²⁺ overload is more related to its function to directly disrupt the BiP-IRE1 α interaction (Fig. 4c, f, g).

Given that BiP is highly promiscuous in its client specificity [86], we could not exclude the possibility that high Ca²⁺ also affects the BiP-PERK/ATF6 interactions. BiP has also been shown to bind Ca²⁺ [87, 88], though the designated Ca²⁺-binding sites have not been identified. It seems that Ca²⁺ binding to BiP helps BiP-substrate interaction, and Ca²⁺-depletion in ER destabilizes the BiP-substrate interaction. For example, Ca²⁺ and ATP have been shown to bind to BiP in a cooperative manner which is essential for the peptide binding and folding abilities of this BiP chaperone [26, 89]. ER Ca²⁺ is required for the binding capacity of BiP for ER-resident SREBP2 and prevents its exit from the ER [53]. Changes in BiP's substrate interaction kinetics are observed within minutes of ER Ca²⁺ depletion [90]. ER Ca²⁺ depletion can cause TCR α protein's dissociation from BiP thus facilitating its exit from ER [26]. Our present results showed that high ER Ca²⁺ level (ER Ca²⁺ overload) disrupts BiP interaction with IRE1 α (Fig. 4c), suggesting that excessive

(See figure on next page.)

Fig. 6 TMCO1 knockdown sensitizes IRE1 α -XBP1 axis to promote cell survival. **a** Representative annexin V-FITC and PI staining in WT or TMCO1 KD cells treated with/without 20 μ M KIRA6 for 24 h followed by flow cytometry. AV, annexin V. **b** The proportion of dead cells was counted in A. Bar graphs represent the mean \pm SEM from three independent assays. **c** Western blotting analysis of proteins in WT and TMCO1 KD cells treated with/without 20 μ M KIRA6 for 24 h. GAPDH was used as a loading control. **d** qRT-PCR analysis of *Xbp1s* in the liver from *Tmco1*^{+/+} and *Tmco1*^{-/-} mice at 2 months of age injected intraperitoneally with TM (2 μ g/g) for 8 h. Each point represents independent animal. Untreated mice, NT; n=8; TM treated mice: n=8. **e** The levels of XBP1s in the livers from *Tmco1*^{+/+} and *Tmco1*^{-/-} mice injected intraperitoneally with TM (2 μ g/g) for 8 h were measured through immunoblotting. GAPDH was used as a loading control. Quantification of the relative expression of XBP1s was shown in the right panel. Bar graphs represent the mean \pm SEM from three independent experiments. Each point represents independent animal. **f** qRT-PCR analysis of *Bloc1s1*, *Bip*, *Chop* in the liver from *Tmco1*^{+/+} and *Tmco1*^{-/-} mice injected intraperitoneally with TM (2 μ g/g) for 8 h. Each point represents independent animal. Untreated mice, NT; n=8; TM treated mice: n=8. n.s., no significance. **g** Representative images of H&E staining of liver tissues from *Tmco1*^{+/+} and *Tmco1*^{-/-} mice injected with Tm for 8 h (magnification \times 200). Scale bar, 100 μ m. Three animals per group were analyzed

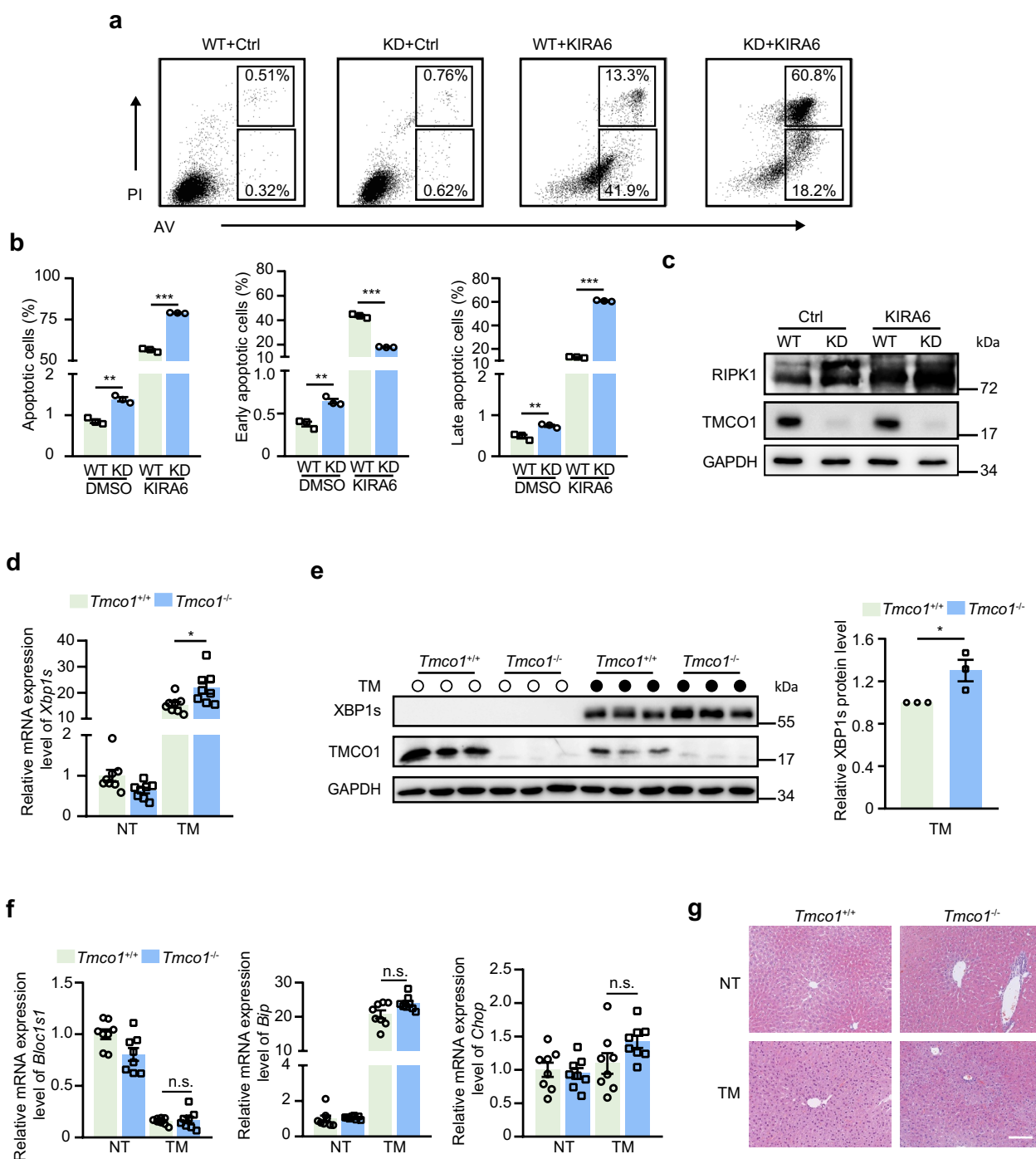


Fig. 6 (See legend on previous page.)

Ca²⁺ binding to BiP also destabilizes BiP-protein interactions. Here, using TMCO1 KD cells, we report a model of UPR regulation in which the three UPR branches are regulated divergently: IRE1α is activated while PERK and ATF6 are attenuated. These data support that TMCO1 knockdown preferentially sensitizes the IRE1α-XBP1

pathway, although the exact mechanism needs further investigation. Therefore, both ER Ca²⁺ overload and Ca²⁺ depletion could cause ER stress response, although they function through distinct mechanisms.

Activation of IRE1α induced by TMCO1 depletion or *Tmco1* knockout appears to be a life-versus-death

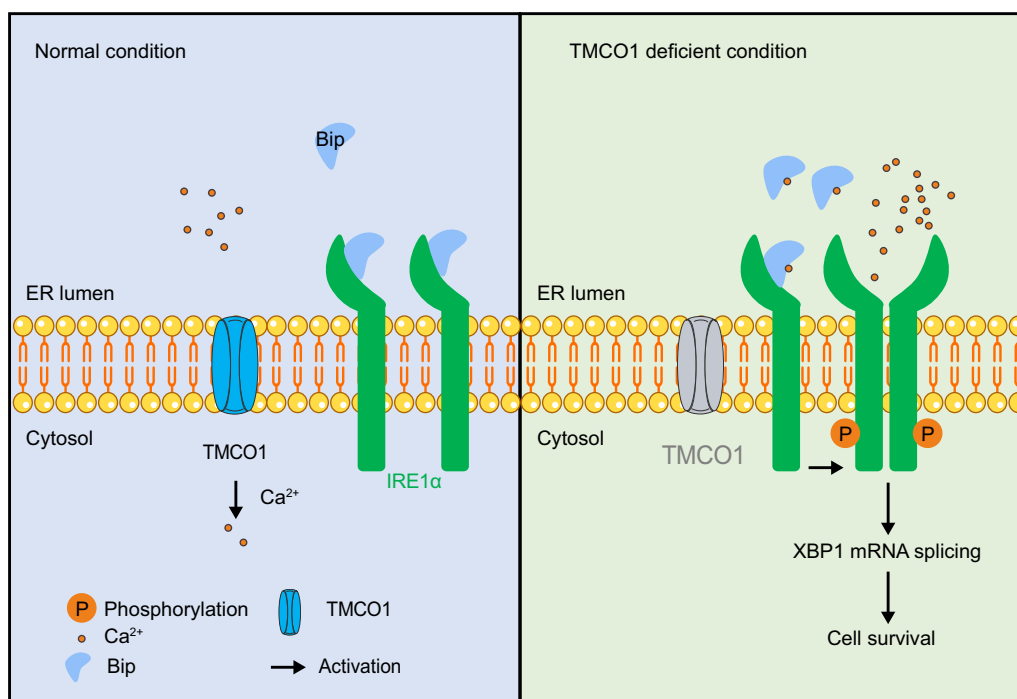


Fig. 7 Graphical Abstract for TMCO1 deficiency-induced the activation of IRE1α-XBP1 axis. Graphical Abstract: under basal conditions, the monomeric inactive state of IRE1α is maintained through the interaction with chaperone Bip. In the case of TMCO1 knockdown, the induced overfilling of Ca²⁺ signaling decreases the interaction between IRE1α and Bip, increases IRE1α dimerization and then promotes cell survival through sensitizing IRE1α-XBP1 axis

determination in both cells and mice. IRE1α has long been identified as a positive regulator of cell survival. Conversely, the repression of IRE1α is related to potentiating apoptosis [71, 91, 92]. Autophosphorylation of IRE1α activates its RNase domain to cleave XBP1 mRNA, producing a potent transcription factor called XBP1s [13]. Target genes of XBP1s encode proteins that promote ER protein folding capacity and quality control [93]. IRE1α improves cell adaptation by enhancing XBP1 mRNA splicing. Moreover, following the formation of high-order clusters, IRE1α can interact with some proteins, including the proapoptotic BCL-2 family members BAX and BAK, the scaffold proteins TRAF2, TRAF6, and RACK1, and STAT3, potentially to regulate apoptosis, inflammation, and proliferation [16, 44, 94–101]. The result that knockdown of TMCO1 resulted in a lower level of XBP1 splicing compared to TG-treated cells, indicates that the activation of IRE1α caused by TMCO1 depletion is in the adaptive UPR stage and is more likely to promote cell survival (Additional file 1e). TMCO1 knockdown could lead to the increase of apoptosis, and the activation of IRE1α induced by ER Ca²⁺ overload is mainly to resist the deterioration from early apoptosis to late apoptosis (Fig. 6a, c).

In summary, this study establishes a model of ER stress caused by ER Ca²⁺ overload and identified TMCO1 as a novel regulator of IRE1α. We define the increased protein stability of IRE1α regulated by ER Ca²⁺ as a new concept of the priming state and provide insights into further understanding of IRE1α activation.

Conclusions

Our findings not only identify TMCO1 as a novel regulator of IRE1α, but also highlight an unexpected role of overload of ER Ca²⁺ in ER stress regulation, which represents a novel model of UPR signaling activation mediated by excess ER Ca²⁺. Given the central role of IRE1α in the regulation of cell fate and in the pathology of various diseases, establishing a causal link between TMCO1 depletion and ER Ca²⁺ overfilling with IRE1α will help the discovery of drugs targeting the UPR signaling.

Materials and methods

Antibodies, chemicals, plasmids, and primers

The sources of antibodies, chemicals, plasmids, and primers used in this study can be found in Additional file 5.

Animals

The *Tmco1*^{+/-} mouse strain (C57BL/6 J) was generated in Shanghai Model Organisms Center, Inc. (Shanghai, China), as described previously [78]. The male wild type, *Tmco1*^{+/+} (C57BL/6 J) or *Tmco1*^{-/-} mice aged 8 weeks were used for all experiments. Mice were housed in a temperature-controlled environment with a 12-h light/dark cycle and free access to water and feed. All animal experiments were approved by the Institute of Zoology Institutional Animal Care and Use Committee.

Cells lines

HeLa cells, TMCO1 KD HeLa cells and HEK-293 T cells were cultured in Dulbecco's modified Eagle's medium (DMEM) with 10% fetal bovine serum (FBS) at 37 °C in a 5% CO₂ environment. TMCO1 KD HeLa cells were described previously [33].

UPRE-mCherry reporter construction

UPRE-mCherry reporter has been previously described, which occurred subsequent to endogenous XBP1 splicing [43]. The UPRE promoter region contains 5 UPR elements (UPREs, 5'-TGACGTGG-3') upstream of the c-fos minimal promoter (-53 to +45 of the human c-fos promoter) [102]. Finally, mCherry was cloned adjacent to UPRE.

Lentivirus production

For lentivirus production, HEK-293 T cells were co-transfected with lentivirus vector and packaging plasmids psPAX2 and pMD.2G using PEI. Following 48–72 h of transfection, lentivirus particles were collected for experiments.

RNA isolation and qRT-PCR

Total RNA from cells or tissues was extracted by TRIzol Reagent (Invitrogen, 15596026). RNA (1 µg) was reverse-transcribed with GoStripTM Reverse Transcription System (Promega, A5001). Quantitative real-time PCR reactions for target genes were performed using Hieff UNICON[®] Universal Blue qPCR SYBR Green Master Mix (YEASON, 11184ES03). *Gapdh* was used as a normalization control for mRNA. The primer sequences are shown in Reagents and Tools Table.

Western blotting assay

Cells or tissues were harvested, washed with phosphate-buffered saline (PBS) and lysed on ice with RIPA buffer (150 mM NaCl, 50 mM Tris-HCl, pH 8.0, 1% NP-40, 0.1% sodium dodecyl sulfate (SDS), and 0.5% sodium deoxycholate) containing 50 mM DTT, 1 mM EDTA, 1 mM PMSE, 1 mM NaF and protease inhibitor cocktail (Roche). Then, lysates were centrifuged at 15,000 rpm for

10 min at 4 °C. The total protein was separated by SDS-PAGE and incubated with primary antibodies for 1 h at room temperature and then at 4 °C overnight. Finally, secondary antibodies conjugated with horseradish peroxidase were incubated for 2 h at room temperature. The bands were visualized by chemiluminescence (Millipore). Density measurements of bands were performed in ImageJ.

Cycloheximide (CHX) chase assay

Cells were treated with 25 µg/ml CHX and harvested at the indicated time points. Lysates were analyzed by 10% SDS-PAGE followed by immunoblotting.

SUnSET assay

SUnSET assay was performed as described previously [42]. Cells were incubated with 10 µg/mL puromycin at 37 °C for 10 min, washed with PBS, and lysed for western blotting with anti-puromycin antibody (Merck, Cat#MABE343).

Immunoprecipitation

Cells were lysed in NETN buffer (100 mM NaCl, 1 mM EDTA, 20 mM Tris-HCl, pH 8.0, 0.5% NP-40) containing protease inhibitor cocktail (Roche). After incubation for 1 h at 4 °C, the total cell lysates were centrifuged at 4 °C. For pulldown of FLAG-tagged proteins, the cell supernatant was incubated with M2 beads (Sigma-Aldrich) at 4 °C overnight with a rotating mixer. The next day, the beads were washed with NETN buffer three times. Samples were separated by 10% SDS-PAGE and analyzed by immunoblotting.

Protein purification

For IRE1α-LD-FLAG protein purification, a total of three 10-cm dishes of HEK-293 T cells expressing IRE1α-LD-FLAG were lysed in NETN buffer containing protease inhibitor cocktail for 45 min at 4 °C. The total cell lysates were centrifuged at 4 °C, and the cell supernatants were incubated with M2 beads (Sigma-Aldrich) overnight at 4 °C with a rotating mixer. The beads were washed with NETN buffer, and then the IRE1α-LD-FLAG proteins were eluted with Flag peptide in buffer B (50 mM HEPES, 75 mM NaCl, 10% glycerol, 1 mM TCEP, pH 7.5). The eluents were concentrated and purified with a centrifugal ultrafiltration tube (Millipore, 0.5 ML 30 KD). Finally, the concentration of purified protein was determined by NanoDrop Spectrophotometer (Thermo-Fisher Scientific).

Pull down assays

For the pulldown assay between GST-BiP-NBD (residues 28–405) [54] and IRE1α-LD-FLAG (residues 1–440) [54],

bacterially purified GST-BiP-NBD immobilized on glutathione Sepharose 4B beads was incubated with IRE1 α -LD-FLAG protein eluents purified from HEK-293 T cells in buffer B with different concentrations of Ca²⁺ at room temperature for 2 h. After that, the beads were washed with buffer B. And then, IRE1 α -LD-FLAG was analyzed by anti-FLAG immunoblotting. Bacterially purified BiP-NBD proteins were visualized by Ponceau S staining.

Intracellular Ca²⁺ measurement

Intracellular Ca²⁺ measurement was performed as described previously [33]. To measure Ca²⁺ content in the ER, cells were loaded with 4 μ M Fura-2 AM (Invitrogen, F1221) and 0.02% pluronic F-127 (Invitrogen, P3000MP) in ECS (140 mM NaCl, 5 mM KCl, 10 mM Glucose, 10 mM HEPES, 2 mM CaCl₂, 1 mM MgCl₂, pH 7.2–7.4) for 40 min at room temperature in the dark. After three washes with ECS, the cells were incubated for another 10 min in ECS buffer for de-esterification. TG (1 μ M) was applied to release Ca²⁺ from the ER in Ca²⁺-free Hank's balanced salt solutions: 140 mM NaCl, 5 mM KCl, 10 mM glucose, 10 mM HEPES, and 1 mM MgCl₂, pH 7.4. Different Ca²⁺ release inducers were applied in the same manner as TG. Ca²⁺ imaging was taken every 3 s with a Nikon inverted microscope (Eclipse TiE) with a 40 \times magnification oil-immersion objective by alternatively excitation at 340 nm and 380 nm. Single-cell Fura-2 images were captured and processed by Metamorph software (version 7.0). The Ca²⁺ level was determined by the 340/380 fluorescence ratio after the Ca²⁺ image background was subtracted. The ER Ca²⁺ content was calculated by the area under the curve induced by the indicated reagents that induce Ca²⁺ release.

Statistical analysis

Data are shown as the mean \pm SEM, and two tailed unpaired Student's *t* test and one-way ANOVA followed by Tukey's multiple comparison test were used for statistical significance analysis. All statistical tests were performed by GraphPad Prism 8.

Abbreviations

ER	Endoplasmic reticulum
TMCO1	Transmembrane and coiled-coil domains 1
CLAC	Ca ²⁺ load-activated Ca ²⁺ channel
IRE1 α /ERN1	Inositol-requiring enzyme 1
XBP1	X-box binding protein 1
BiP	Binding immunoglobulin protein
TG	Thapsigargin
ERAD	ER-associated degradation
SERCA	Sarco-/endoplasmic-reticulum Ca ²⁺ -ATPase
CFTD	Cerebrofaciothoracic dysplasia
miGer	MKate-linker-G-CEPIA1er
qRT-PCR	Quantitative real-time polymerase chain reaction

Supplementary Information

The online version contains supplementary material available at <https://doi.org/10.1186/s13578-023-01062-y>.

Additional file 1. TMCO1 KD leads to the over-activation of IRE1 α and regulates RIDD. Related to Fig. 1. (a) IRE1 α , p-IRE1 α , XBP1s, BiP and CHOP levels were analyzed by immunoblotting in the WT or TMCO1-knockdown cells. GAPDH was used as a loading control. Relative quantification of each protein was shown in the right panel. Bar graphs represent the mean \pm SEM from three independent experiments. ***P* < 0.01, n.s., no significance. (b–d) qRT-PCR analysis of Bip (b), Chop (c) and SPARC (d) mRNA levels in WT or TMCO1 KD cells. Data are shown as mean \pm SEM from three independent experiments. n.s., no significance, ****P* < 0.001. (e) qRT-PCR analysis of XBP1 mRNA splicing in WT or TMCO1 KD cells treated with 1 μ M TG for the indicated times. Bar graphs represent the mean \pm SEM from three independent assays. **P* < 0.05; ***P* < 0.01, n.s., no significance. (f) Western blotting analysis of mCherry and XBP1s levels in the HEK-293 T expressing UPRE-mCherry treated with 1 μ M TG along with/without 50 μ M 4 μ 8C for 6 h. GAPDH was used as a loading control. Quantification of the relative protein levels are shown in the right panel. Bar graphs represent the mean \pm SEM from three independent experiments. ***P* < 0.01, ****P* < 0.001, n.s., no significance. (g) Western blotting analysis of TMCO1 levels after TMCO1 KD in the HEK-293 T. GAPDH was used as a loading control. Relative quantification of each protein was shown in the down panel. Bar graphs represent the mean \pm SEM from three independent experiments. **P* < 0.05; ****P* < 0.001. (h) 1 μ M TG-triggered Ca²⁺ transients in WT (purple trace line, n = 300) and TMCO1 KD (red trace line, n = 300) HEK-293 T cells. Each trace line in H is an average of Ca²⁺ responses in each group. Right panel, statistical analysis of the average peak area of TG-triggered Ca²⁺ mobilization curves. ****P* < 0.001. (i) IRE1 α , XBP1s, TMCO1 levels were analyzed by immunoblotting in the WT or TMCO1 KD HEK-293 T cells. GAPDH was used as a loading control. Relative quantification of each protein was shown in the right panel. Bar graphs represent the mean \pm SEM from three independent experiments. ***P* < 0.01; ****P* < 0.001.

Additional file 2. Effects of TM and DTT on the ER Ca²⁺ transients. Related to Fig. 2. (a) Assessment of protein synthesis in WT HeLa cells treated with or without BAPTA-AM (100 μ M, 2 h) by SUNSET. Data represent as the mean protein intensity normalized to GAPDH \pm SEM from 3 independent experiments. ***P* < 0.01. (b) 3 μ g/ml TM or 1 μ M TG-triggered Ca²⁺ transients in WT (purple trace line, n = 45) and TMCO1 KD (red trace line, n = 37) cells. Each trace line in B is an average of Ca²⁺ responses in each group. Right panel, statistical analysis of the average peak area of TG-triggered Ca²⁺ mobilization curves. ****P* < 0.001. (c) 5 mM DTT or 1 μ M TG-triggered Ca²⁺ transients in WT (purple trace line, n = 63) and TMCO1 KD (red trace line, n = 61) cells. Each trace line in C is an average of Ca²⁺ responses in each group. Right panel, statistical analysis of the average peak area of TG-triggered Ca²⁺ mobilization curves. ****P* < 0.001.

Additional file 3. TMCO1 knockdown leads to the overload of ER Ca²⁺ store. Related to Fig. 3. (a) 100 μ M Cch-triggered Ca²⁺ transients in WT (purple trace line, n = 33) and TMCO1 KD (red trace line, n = 25) HeLa cells. Each trace line is an average of Ca²⁺ responses in each group. Right panel, statistical analysis of the average peak area of Cch-triggered Ca²⁺ mobilization curves. Bar graphs represent the mean \pm SEM from three independent assays. ****P* < 0.001. (b) 1 μ M iono-triggered Ca²⁺ transients in WT (purple trace line, n = 42) and TMCO1 KD (red trace line, n = 57) HeLa cells. Each trace line is an average of Ca²⁺ responses in each group. Right panel, statistical analysis of the average peak area of iono-triggered Ca²⁺ mobilization curves. Bar graphs represent the mean \pm SEM from three independent assays. ****P* < 0.001. (c) 100 μ M ATP-triggered Ca²⁺ transients in WT (purple trace line, n = 41), TMCO1 KD (red trace line, n = 44) cells. Each trace line is an average of Ca²⁺ responses in each group. Right panel, statistical analysis of the average peak area of ATP-triggered Ca²⁺ mobilization curves. Bar graphs represent the mean \pm SEM from three independent assays. ****P* < 0.001. (d) The resting G-CEPIA1er fluorescence ratio signals were detected in WT (n = 454) or TMCO1 KD (n = 540) cells. Bar graphs represent the mean \pm SEM from three independent assays. ****P* < 0.001.

Additional file 4. TMCO1 KD activates IRE1 α to prevent cell death. Related to Fig. 6. (a) qRT-PCR analysis of Xbp1s in the liver from 2-month-old WT

mice injected intraperitoneally with TM (2 µg/g) for the indicated times. Bar graphs represent the mean ± SEM. Each point represents independent animal. ** $P < 0.01$, *** $P < 0.001$. (b) Western blotting analysis and quantification of proteins in WT mice injected with TM for the indicated times. GAPDH was used as a loading control. Data represent as the mean protein intensity normalized to GAPDH ± SEM from 3 independent experiments. Each point represents independent animal. * $P < 0.05$, n.s., no significance. (c) Picrosirius red staining of liver tissues from *Tmco1*^{+/+} and *Tmco1*^{-/-} mice injected with TM (magnification ×200). Scale bar, 100 µm. Three animals per group were analyzed. (d) Western blotting analyses of proteins extracted from liver tissues of *Tmco1*^{-/-} mice and *Tmco1*^{+/+} mice at 8 months of age (three mice per group). GAPDH is used as a loading control. Data represent as the mean protein intensity normalized to GAPDH ± SEM from 3 independent experiments. ** $P < 0.01$.

Additional file 5: Table S1. The sources of antibodies used in this study. **Table S2.** The sources of plasmids used in this study. **Table S3.** The sources of primers used in this study. **Table S4.** The sources of chemicals used in this study.

Acknowledgements

We thank Dr Youjun Wang at Beijing Normal University for kindly providing mKate-linker-G-CEPIA1er constructs, Dr Likun Wang at Institute of Biophysics Chinese Academy of Sciences for providing IRE1α knockout cells, and Dr Yong Liu at Wuhan University for providing Flag-IRE1α constructs. We thank Tianjiao Feng for providing the data calculation.

Author contributions

SZ designed and performed most of the experiments with help from HF and DJ. KY, S-TW, Y-XZ, and YW collected samples and assisted in the cell experiments. T-ST and CG supervised the whole project; SZ, HL, CG, and T-ST wrote the manuscript with input from all authors. All authors read and approved the final manuscript.

Funding

This work was supported by National Natural Science Foundation of China 82030033 (T.-S.T.), 92254301 (T.-S.T.), 81921006 (T.-S.T.), 31970740 (C.G.), 32070780 (H.L.), and the State Key Laboratory of Membrane Biology.

Availability of data and materials

Data are available upon reasonable request.

Declarations

Ethics approval and consent to participate

All experimental procedures were in full compliance with the Regulations for the Care and Use of Laboratory Animals by the Ministry of Science and Technology of China and with the Institute of Zoology's Guidelines for the Care and Use of Laboratory Animals. The experimental protocols were approved by the Animal Care and Use Committee at the Institute of Zoology, Chinese Academy of Sciences (Permission Number: IOZ-13049).

Consent for publication

Not applicable.

Competing interests

All authors declare that they have no competing interests.

Received: 10 February 2023 Accepted: 26 May 2023

Published online: 03 July 2023

References

- Sepulveda D, Rojas-Rivera D, Rodriguez DA, Groenendyk J, Kohler A, Lebeaupin C, et al. Interactome screening identifies the ER luminal chaperone Hsp47 as a regulator of the unfolded protein response transducer IRE1α. *Mol Cell*. 2018;69(238–52):e7.
- Xu C, Bailly-Maitre B, Reed JC. Endoplasmic reticulum stress: cell life and death decisions. *J Clin Invest*. 2005;115:2656–64.
- Walter P, Ron D. The unfolded protein response: from stress pathway to homeostatic regulation. *Science*. 2011;334:1081–6.
- You K, Wang L, Chou CH, Liu K, Nakata T, Jaiswal A, et al. QRIH1 dictates the outcome of ER stress through transcriptional control of proteostasis. *Science*. 2021;371(6524):eabb6896.
- Bertolotti A, Zhang Y, Hendershot LM, Harding HP, Ron D. Dynamic interaction of BiP and ER stress transducers in the unfolded-protein response. *Nat Cell Biol*. 2000;2:326–32.
- Ghemrawi R, Battaglia-Hsu SF, Arnold C. Endoplasmic reticulum stress in metabolic disorders. *Cells*. 2018;7(6):63–97.
- Kny M, Fielitz J. Hidden agenda—the involvement of endoplasmic reticulum stress and unfolded protein response in inflammation-induced muscle wasting. *Front Immunol*. 2022;13:878755–80.
- Ochoa CD, Wu RF, Terada LS. ROS signaling and ER stress in cardiovascular disease. *Mol Aspects Med*. 2018;63:18–29.
- Ma K, Vattem KM, Wek RC. Dimerization and release of molecular chaperone inhibition facilitate activation of eukaryotic initiation factor-2 kinase in response to endoplasmic reticulum stress. *J Biol Chem*. 2002;277:18728–35.
- Wang XZ, Harding HP, Zhang Y, Jolicoeur EM, Kuroda M, Ron D. Cloning of mammalian Ire1 reveals diversity in the ER stress responses. *EMBO J*. 1998;17:5708–17.
- Cox JS, Shamu CE, Walter P. Transcriptional induction of genes encoding endoplasmic reticulum resident proteins requires a transmembrane protein kinase. *Cell*. 1993;73:1197–206.
- Hetz C, Martinon F, Rodriguez D, Glimcher LH. The unfolded protein response: integrating stress signals through the stress sensor IRE1α. *Physiol Rev*. 2011;91:1219–43.
- Yoshida H, Matsui T, Yamamoto A, Okada T, Mori K. XBP1 mRNA is induced by ATF6 and spliced by IRE1 in response to ER stress to produce a highly active transcription factor. *Cell*. 2001;107:881–91.
- Han J, Kaufman RJ. Physiological/pathological ramifications of transcription factors in the unfolded protein response. *Genes Dev*. 2017;31:1417–38.
- Shoulders MD, Ryno LM, Genereux JC, Moresco JJ, Tu PG, Wu C, et al. Stress-independent activation of XBP1s and/or ATF6 reveals three functionally diverse ER proteostasis environments. *Cell Rep*. 2013;3:1279–92.
- Urano F, Wang X, Bertolotti A, Zhang Y, Chung P, Harding HP, Ron D. Coupling of stress in the ER to activation of JNK protein kinases by transmembrane protein kinase IRE1. *Science*. 2000;287:664–6.
- Grandjean JMD, Wiseman RL. Small molecule strategies to harness the unfolded protein response: where do we go from here? *J Biol Chem*. 2020;295:15692–711.
- Gaut JR, Hendershot LM. The modification and assembly of proteins in the endoplasmic reticulum. *Curr Opin Cell Biol*. 1993;5:589–95.
- Travers KJ, Patil CK, Wodicka L, Lockhart DJ, Weissman JS, Walter P. Functional and genomic analyses reveal an essential coordination between the unfolded protein response and ER-associated degradation. *Cell*. 2000;101:249–58.
- Coe H, Michalak M. Calcium binding chaperones of the endoplasmic reticulum. *Gen Physiol Biophys*. 2009;28:F96–103.
- Lebeau PF, Platko K, Byun JH, Austin RC. Calcium as a reliable marker for the quantitative assessment of endoplasmic reticulum stress in live cells. *J Biol Chem*. 2021;296:100779–87.
- Lee JH, Han JH, Kim H, Park SM, Joe EH, Jou I. Parkinson's disease-associated LRRK2-G2019S mutant acts through regulation of SERCA activity to control ER stress in astrocytes. *Acta Neuropathol Commun*. 2019;7:68–86.
- Wong WL, Brostrom MA, Kuznetsov G, Gmitter-Yellen D, Brostrom CO. Inhibition of protein synthesis and early protein processing by thapsigargin in cultured cells. *Biochem J*. 1993;289(Pt 1):71–9.
- Paredes RM, Bollo M, Holstein D, Lechleiter JD. Luminal Ca²⁺ depletion during the unfolded protein response in *Xenopus* oocytes: cause and consequence. *Cell Calcium*. 2013;53:286–96.
- Karagoz GE, Acosta-Alvear D, Walter P. The unfolded protein response: detecting and responding to fluctuations in the protein-folding capacity of the endoplasmic reticulum. *Cold Spring Harb Perspect Biol*. 2019;11(9):a033886.

26. Preissler S, Rato C, Yan Y, Perera LA, Czako A, Ron D. Calcium depletion challenges endoplasmic reticulum proteostasis by destabilising BiP-substrate complexes. *Elife*. 2020;9:e62601.
27. Bezprozvanny I. Calcium signaling and neurodegenerative diseases. *Trends Mol Med*. 2009;15:89–100.
28. Bezprozvanny I, Mattson MP. Neuronal calcium mishandling and the pathogenesis of Alzheimer's disease. *Trends Neurosci*. 2008;31:454–63.
29. Chan CS, Gertler TS, Surmeier DJ. Calcium homeostasis, selective vulnerability and Parkinson's disease. *Trends Neurosci*. 2009;32:249–56.
30. Surmeier DJ, Halliday GM, Simuni T. Calcium, mitochondrial dysfunction and slowing the progression of Parkinson's disease. *Exp Neurol*. 2017;298:202–9.
31. Surmeier DJ, Obeso JA, Halliday GM. Selective neuronal vulnerability in Parkinson disease. *Nat Rev Neurosci*. 2017;18:101–13.
32. Fischer TT, Ehrlich BE. Wolfram syndrome: a monogenic model to study diabetes mellitus and neurodegeneration. *Curr Opin Physiol*. 2020;17:115–23.
33. Wang QC, Zheng Q, Tan H, Zhang B, Li X, Yang Y, et al. TMCO1 Is an ER Ca(2+) Load-Activated Ca(2+) Channel. *Cell*. 2016;165:1454–66.
34. Xin B, Puffenberger EG, Turben S, Tan H, Zhou A, Wang H. Homozygous frameshift mutation in TMCO1 causes a syndrome with craniofacial dysmorphism, skeletal anomalies, and mental retardation. *Proc Natl Acad Sci U S A*. 2010;107:258–63.
35. Li J, Liu C, Li Y, Zheng Q, Xu Y, Liu B, et al. TMCO1-mediated Ca(2+) leak underlies osteoblast functions via CaMKII signaling. *Nat Commun*. 2019;10:1589–602.
36. Yang K-Y, Zhao S, Feng H, Shen J, Chen Y, Wang S-T, et al. Ca2+ homeostasis maintained by TMCO1 underlies corpus callosum development via ERK signaling. *Cell Death Dis*. 2022. <https://doi.org/10.1038/s41419-022-05131-x>.
37. Madhavan A, Kok BP, Rius B, Grandjean JMD, Alabi A, Albert V, et al. Pharmacologic IRE1/XBP1s activation promotes systemic adaptive remodeling in obesity. *Nat Commun*. 2022;13:608–16.
38. Maurel M, Chevet E, Tavernier J, Gerlo S. Getting RIDD of RNA: IRE1 in cell fate regulation. *Trends Biochem Sci*. 2014;39:245–54.
39. Bright MD, Itzhak DN, Wardell CP, Morgan GJ, Davies FE. Cleavage of BLOC1S1 mRNA by IRE1 is sequence specific, temporally separate from XBP1 splicing, and dispensable for cell viability under acute endoplasmic reticulum stress. *Mol Cell Biol*. 2015;35:2186–202.
40. Hollien J, Weissman JS. Decay of endoplasmic reticulum-localized mRNAs during the unfolded protein response. *Science*. 2006;313:104–7.
41. Morita S, Villalta SA, Feldman HC, Register AC, Rosenthal W, Hoffmann-Petersen IT, et al. Targeting ABL-IRE1alpha signaling spares ER-stressed pancreatic beta cells to reverse autoimmune diabetes. *Cell Metab*. 2017;25(883–97):e8.
42. Li T, Zhao H, Guo G, Xia S, Wang L. VMP1 affects endoplasmic reticulum stress sensitivity via differential modulation of the three unfolded protein response arms. *Cell Rep*. 2023;42:112209–32.
43. Adamson B, Norman TM, Jost M, Cho MY, Nunez JK, Chen Y, et al. A multiplexed single-cell CRISPR screening platform enables systematic dissection of the unfolded protein response. *Cell*. 2016;167(1867–82):e21.
44. Qiu Q, Zheng Z, Chang L, Zhao YS, Tan C, Dandekar A, et al. Toll-like receptor-mediated IRE1alpha activation as a therapeutic target for inflammatory arthritis. *EMBO J*. 2013;32:2477–90.
45. Paschen W, Hotop S, Aufenberg C. Loading neurons with BAPTA-AM activates xbp1 processing indicative of induction of endoplasmic reticulum stress. *Cell Calcium*. 2003;33:83–9.
46. Sehgal P, Szalai P, Olesen C, Praetorius HA, Nissen P, Christensen SB, Engedal N, Moller JV. Inhibition of the sarco/endoplasmic reticulum (ER) Ca(2+)-ATPase by thapsigargin analogs induces cell death via ER Ca(2+) depletion and the unfolded protein response. *J Biol Chem*. 2017;292:19656–73.
47. Maity S, Rajkumar A, Matai L, Bhat A, Ghosh A, Agam G, et al. Oxidative homeostasis regulates the response to reductive endoplasmic reticulum stress through translation control. *Cell Rep*. 2016;16:851–65.
48. Li J, Wang L, Chen Y, Yang Y, Liu J, Liu K, et al. Visible light excited ratio-metric-GECs for long-term in-cellulo monitoring of calcium signals. *Cell Calcium*. 2020;87:102165–71.
49. Li X, Sun S, Appathurai S, Sundaram A, Plumb R, Mariappan M. A Molecular mechanism for turning off IRE1alpha signaling during endoplasmic reticulum stress. *Cell Rep*. 2020;33:108563–93.
50. Liu CY, Schroder M, Kaufman RJ. Ligand-independent dimerization activates the stress response kinases IRE1 and PERK in the lumen of the endoplasmic reticulum. *J Biol Chem*. 2000;275:24881–5.
51. Volmer R, van der Ploeg K, Ron D. Membrane lipid saturation activates endoplasmic reticulum unfolded protein response transducers through their transmembrane domains. *Proc Natl Acad Sci U S A*. 2013;110:4628–33.
52. Williams DB. Beyond lectins: the calnexin/calreticulin chaperone system of the endoplasmic reticulum. *J Cell Sci*. 2006;119:615–23.
53. Lebeau PF, Byun JH, Platko K, Saliba P, Sguazzin M, MacDonald ME, et al. Caffeine blocks SREBP2-induced hepatic PCSK9 expression to enhance LDLR-mediated cholesterol clearance. *Nat Commun*. 2022;13:770–86.
54. Carrara M, Prisci F, Nowak PR, Kopp MC, Ali MM. Noncanonical binding of BiP ATPase domain to Ire1 and Perk is dissociated by unfolded protein CH1 to initiate ER stress signaling. *Elife*. 2015;4:e03522.
55. Kopp MC, Nowak PR, Larburu N, Adams CJ, Ali MM. In vitro FRET analysis of IRE1 and BiP association and dissociation upon endoplasmic reticulum stress. *Elife*. 2018;7:e30257.
56. Suzuki J, Kanemaru K, Iino M. Genetically encoded fluorescent indicators for organellar calcium imaging. *Biophys J*. 2016;111:1119–31.
57. Bootman MD, Collins TJ, Mackenzie L, Roderick HL, Berridge MJ, Peppiatt CM. 2-aminoethoxydiphenyl borate (2-APB) is a reliable blocker of store-operated Ca2+ entry but an inconsistent inhibitor of InsP3-induced Ca2+ release. *FASEB J*. 2002;16:1145–50.
58. Szeberenyi J. The effect of actinomycin D on RNA metabolism in human cells. *Biochem Mol Biol Educ*. 2006;34:50–1.
59. Lu DF, Wang YS, Li C, Wei GJ, Chen R, Dong DM, Yao M. Actinomycin D inhibits cell proliferations and promotes apoptosis in osteosarcoma cells. *Int J Clin Exp Med*. 2015;8:1904–11.
60. Zheng S, Zhao D, Hou G, Zhao S, Zhang W, Wang X, et al. iASPP suppresses Gp78-mediated TMCO1 degradation to maintain Ca(2+) homeostasis and control tumor growth and drug resistance. *Proc Natl Acad Sci U S A*. 2022;119:e2111380119.
61. Sun S, Shi G, Sha H, Ji Y, Han X, Shu X, et al. IRE1alpha is an endogenous substrate of endoplasmic-reticulum-associated degradation. *Nat Cell Biol*. 2015;17:1546–55.
62. Sundaram A, Plumb R, Appathurai S, Mariappan M. The Sec61 translocon limits IRE1alpha signaling during the unfolded protein response. *Elife*. 2017;6:e27187.
63. Liu H, Li X, Ning G, Zhu S, Ma X, Liu X, et al. The Machado-Joseph disease deubiquitinase ataxin-3 regulates the stability and apoptotic function of p53. *PLoS Biol*. 2016;14:e2000733.
64. Kim SH, Kwon DY, Kwak JH, Lee S, Lee YH, Yun J, Son TG, Jung YS. Tunicamycin-induced ER stress is accompanied with oxidative stress via abrogation of sulfur amino acids metabolism in the liver. *Int J Mol Sci*. 2018;19(12):4114–26.
65. Marciniak SJ, Yun CY, Oyadomari S, Novoa I, Zhang Y, Jungreis R, Nagata K, Harding HP, Ron D. CHOP induces death by promoting protein synthesis and oxidation in the stressed endoplasmic reticulum. *Genes Dev*. 2004;18:3066–77.
66. Kriegermeier A, Hyon A, Sommars M, Hubchak S, LeCuyer B, Liu XY, Barish G, Green RM. Hepatic X-box binding protein 1 and unfolded protein response is impaired in weanling mice with resultant hepatic injury. *Hepatology*. 2021;74:3362–75.
67. Liu CZ, Zhou B, Meng MY, Zhao WJ, Wang DM, Yuan YW, et al. FOXA3 induction under endoplasmic reticulum stress contributes to non-alcoholic fatty liver disease. *J Hepatol*. 2021;75:150–62.
68. Yang Y, Chen H, Wan Y, Dong DD, Wang XF, Yao SH, et al. Protective role of hepassocin against hepatic endoplasmic reticulum stress in mice. *Int J Mol Sci*. 2022;23(21):13325–45.
69. Duran-Aniotz C, Poblete N, Rivera-Krstulovic C, Ardiles AO, Diaz ML, Tamburini G, et al. The unfolded protein response transcription factor XBP1s ameliorates Alzheimer's disease by improving synaptic function and proteostasis. *Mol Ther*. 2023. <https://doi.org/10.1016/j.jymth.2023.03.028>.
70. Hotamisligil GS. Endoplasmic reticulum stress and atherosclerosis. *Nat Med*. 2010;16:396–9.
71. Chen Y, Brandizzi F. IRE1: ER stress sensor and cell fate executor. *Trends Cell Biol*. 2013;23:547–55.

72. Krebs J, Agellon LB, Michalak M. Ca(2+) homeostasis and endoplasmic reticulum (ER) stress: an integrated view of calcium signaling. *Biochem Biophys Res Commun*. 2015;460:114–21.
73. Michalak M, Robert Parker JM, Opas M. Ca2+ signaling and calcium binding chaperones of the endoplasmic reticulum. *Cell Calcium*. 2002;32:269–78.
74. Ma Y, Hendershot LM. ER chaperone functions during normal and stress conditions. *J Chem Neuroanat*. 2004;28:51–65.
75. Mekahli D, Bultynck G, Parys JB, De Smedt H, Missiaen L. Endoplasmic-reticulum calcium depletion and disease. *Cold Spring Harb Perspect Biol*. 2011;3(6):a004317.
76. Ding WX, Ni HM, Gao W, Hou YF, Melan MA, Chen X, Stolz DB, Shao ZM, Yin XM. Differential effects of endoplasmic reticulum stress-induced autophagy on cell survival. *J Biol Chem*. 2007;282:4702–10.
77. Lebeau P, Al-Hashimi A, Sood S, Lhotak S, Yu P, Gyulay G, et al. Endoplasmic reticulum stress and Ca2+ depletion differentially modulate the sterol regulatory protein PCSK9 to control lipid metabolism. *J Biol Chem*. 2017;292:1510–23.
78. Sun Z, Zhang H, Wang X, Wang QC, Zhang C, Wang JQ, et al. TMCO1 is essential for ovarian follicle development by regulating ER Ca(2+) store of granulosa cells. *Cell Death Differ*. 2018;25:1686–701.
79. Amin-Wetzel N, Neidhardt L, Yan Y, Mayer MP, Ron D. Unstructured regions in IRE1alpha specify BiP-mediated destabilisation of the luminal domain dimer and repression of the UPR. *Elife*. 2019;8:e50793.
80. Amin-Wetzel N, Saunders RA, Kamphuis MJ, Rato C, Preissler S, Harding HP, Ron D. A J-protein Co-chaperone recruits BiP to monomerize IRE1 and repress the unfolded protein response. *Cell*. 2017;171(1625–37):e13.
81. Wada I, Rindress D, Cameron PH, Ou WJ, Doherty JJ 2nd, Louvard D, et al. SSR alpha and associated calnexin are major calcium binding proteins of the endoplasmic reticulum membrane. *J Biol Chem*. 1991;266:19599–610.
82. Baksh S, Michalak M. Expression of calreticulin in *Escherichia coli* and identification of its Ca2+ binding domains. *J Biol Chem*. 1991;266:21458–65.
83. Van PN, Peter F, Soling HD. Four intracisternal calcium-binding glycoproteins from rat liver microsomes with high affinity for calcium. No indication for calsequestrin-like proteins in inositol 1,4,5-trisphosphate-sensitive calcium sequestering rat liver vesicles. *J Biol Chem*. 1989;264:17494–501.
84. Macer DR, Koch GL. Identification of a set of calcium-binding proteins in reticuloplasm, the luminal content of the endoplasmic reticulum. *J Cell Sci*. 1988;91(Pt 1):61–70.
85. Shen J, Chen X, Hendershot L, Prywes R. ER stress regulation of ATF6 localization by dissociation of BiP/GRP78 binding and unmasking of Golgi localization signals. *Dev Cell*. 2002;3:99–111.
86. Flynn GC, Pohl J, Flocco MT, Rothman JE. Peptide-binding specificity of the molecular chaperone BiP. *Nature*. 1991;353:726–30.
87. Lamb HK, Mee C, Xu W, Liu L, Blond S, Cooper A, Charles IG, Hawkins AR. The affinity of a major Ca2+ binding site on GRP78 is differentially enhanced by ADP and ATP. *J Biol Chem*. 2006;281:8796–805.
88. Lievremon J, Rizzuto R, Hendershot L, Meldolesi J. BiP, a major chaperone protein of the endoplasmic reticulum lumen, plays a direct and important role in the storage of the rapidly exchanging pool of Ca2+. *J Biol Chem*. 1997;272:30873–9.
89. Yang J, Nune M, Zong Y, Zhou L, Liu Q. Close and allosteric opening of the polypeptide-binding site in a human Hsp70 chaperone BiP. *Structure*. 2015;23:2191–203.
90. Preissler S, Chambers JE, Crespillo-Casado A, Avezov E, Miranda E, Perez J, Hendershot LM, Harding HP, Ron D. Physiological modulation of BiP activity by trans-protomer engagement of the interdomain linker. *Elife*. 2015;4:e08961.
91. Upton JP, Wang L, Han D, Wang ES, Huskey NE, Lim L, et al. IRE1alpha cleaves select microRNAs during ER stress to derepress translation of proapoptotic Caspase-2. *Science*. 2012;338:818–22.
92. Han D, Lerner AG, Vande Walle L, Upton JP, Xu W, Hagen A, Backes BJ, Oakes SA, Papa FR. IRE1alpha kinase activation modes control alternate endoribonuclease outputs to determine divergent cell fates. *Cell*. 2009;138:562–75.
93. Lee AH, Iwakoshi NN, Glimcher LH. XBP-1 regulates a subset of endoplasmic reticulum resident chaperone genes in the unfolded protein response. *Mol Cell Biol*. 2003;23:7448–59.
94. Korennykh AV, Egea PF, Korostelev AA, Finer-Moore J, Zhang C, Shokat KM, Stroud RM, Walter P. The unfolded protein response signals through high-order assembly of Ire1. *Nature*. 2009;457:687–93.
95. Li H, Korennykh AV, Behrman SL, Walter P. Mammalian endoplasmic reticulum stress sensor IRE1 signals by dynamic clustering. *Proc Natl Acad Sci U S A*. 2010;107:16113–8.
96. Woehlbier U, Hetz C. Modulating stress responses by the UPProsome: a matter of life and death. *Trends Biochem Sci*. 2011;36:329–37.
97. Hetz C, Bernasconi P, Fisher J, Lee AH, Bassik MC, Antonsson B, et al. Proapoptotic BAX and BAK modulate the unfolded protein response by a direct interaction with IRE1alpha. *Science*. 2006;312:572–6.
98. Qiu Y, Mao T, Zhang Y, Shao M, You J, Ding Q, et al. A crucial role for RACK1 in the regulation of glucose-stimulated IRE1alpha activation in pancreatic beta cells. *Sci Signal*. 2010;3:ra7.
99. Liu Y, Shao M, Wu Y, Yan C, Jiang S, Liu J, et al. Role for the endoplasmic reticulum stress sensor IRE1alpha in liver regenerative responses. *J Hepatol*. 2015;62:590–8.
100. Huang S, Xing Y, Liu Y. Emerging roles for the ER stress sensor IRE1alpha in metabolic regulation and disease. *J Biol Chem*. 2019;294:18726–41.
101. Hetz C, Glimcher LH. Fine-tuning of the unfolded protein response: assembling the IRE1alpha interactome. *Mol Cell*. 2009;35:551–61.
102. Wang Y, Shen J, Arenzana N, Tirasophon W, Kaufman RJ, Prywes R. Activation of ATF6 and an ATF6 DNA binding site by the endoplasmic reticulum stress response. *J Biol Chem*. 2000;275:27013–20.

Publisher's Note

Springer Nature remains neutral with regard to jurisdictional claims in published maps and institutional affiliations.

Ready to submit your research? Choose BMC and benefit from:

- fast, convenient online submission
- thorough peer review by experienced researchers in your field
- rapid publication on acceptance
- support for research data, including large and complex data types
- gold Open Access which fosters wider collaboration and increased citations
- maximum visibility for your research: over 100M website views per year

At BMC, research is always in progress.

Learn more biomedcentral.com/submissions

